Quantitative Comparison of Channel-belt Dimensions, Internal Architecture and Characteristics of Two Fluvial Systems in Sequence 1, Ferron Notom Delta, South-Central Utah, U.S.A.

A Thesis

Presented to

the Faculty of the Department of Earth and Atmospheric Sciences

University of Houston

In Partial Fulfillment

of the Requirements for the Degree

Masters of Science

By

Omar A. Montes

May 2013

Quantitative Comparison of Channel-belt Dimensions, Internal Architecture and Characteristics of Two Fluvial Systems in Sequence 1, Ferron Notom Delta, South-Central Utah, U.S.A.

Omar A. Montes

APPROVED:

Dr. Janok P. Bhattacharya, Advisor

Dr. William R. Dupre, Committee Member

Dr. Mark D. Barton, Committee Member

Dean, College of Natural Science and Mathematics

ACKNOWLEDGEMENTS

First and foremost, I would like to thank God for blessing me with the opportunity to obtain this degree. I committed this task to you, and you were faithful to your word and allowed my plans to succeed. I will forever thank you for giving me the strength and knowledge to make this task come to pass.

I would like to thank my advisor Dr. Janok Bhattacharya for his help and guidance with this task. He has taught me a lot and has pushed me to become a better geologist in the classroom and in the field. I had a very difficult start in grad school, but I thank you for being patient with me and not giving up on me. I would also like to thank my committee members Dr. William Dupre and Dr. Mark Barton for their help and feedback. Their passion for geology and knowledge is absolutely amazing.

I would also like to thank my research partners Oyebode Famubode and Danfix D'Souza. I cannot put into words how truly grateful I am to have met and have worked with both you guys. Both you guys motivated me and encouraged me to keep going during the tough times. I thank you both for the advice and the great memories we made during our time in Utah. I would also like to thank Yangyang Li for taking time out of his schedule to help me in the field.

Last but not least, I would like to give a special thanks to my father Julio Montes, my mother Maritza Montes, and my two brothers, Christian Montes and Richard Montes. You all mean the world to me and I thank you from the bottom of my heart for all of your love and support, not only throughout my educational career, but throughout life. I am truly blessed and grateful to have you all in my life and I dedicate all of my accomplishments to you all.

Quantitative Comparison of Channel-belt Dimensions, Internal Architecture and Characteristics of Two Fluvial Systems in Sequence 1, Ferron Notom Delta, South-Central Utah, U.S.A.

An Abstract of a Thesis

Presented to

the Faculty of the Department of Earth and Atmospheric Sciences

University of Houston

In Partial Fulfillment

of the Requirements for the Degree

Masters of Science

By

Omar A. Montes

May 2013

Abstract

The geometry, proportion, and spatial distribution of fluvial deposits are critical components in subsurface reservoir analysis, but their prediction can be difficult. This study describes and compares an amalgamated, high sandstone/mudstone interval, channel-belt to underlying isolated, low sandstone/mudstone interval, channel-belts within outcrops of the Cretaceous Ferron Sandstone Member of the Mancos Shale Formation in south-central Utah, U.S.A.

Using an oblique to mean paleocurrent direction cross section, photomosaics, and GPS readings at respective channel-belt margins, the width (W), thickness (T), and width/thickness ratio (W/T) of 12 channel-belts were documented. The amalgamated channel-belt demonstrates a minimum true channel-belt width of ~2.8 km, an average channel-belt thickness of 2.5m, and a minimum W/T ratio of ~1130. The isolated channel-belts range from approximately 40m up to 245m in true channel-belt width, 1.1m up to 5m in channel-belt thickness, and W/T ratios ranging from 25 to 175. The amalgamated channel-belt was formed by low sinuosity braided channels; whereas the isolated channel-belts were most likely laterally migrating meandering distributary channels in the upper delta plain.

Using channel-belt dimensions, we determined that there is not a consistent systematic change in channel-belt dimensions relating changes in dimensions to their positioning within a sequence. However, there does appear to be a systematic change in the sandstone/mudstone proportion, where confined valley fill deposits result in high sandstone/mudstone proportions. This is followed by the out-of-valley deposits which are predominantly mudstone with isolated, highly sinuous fluvial deposits, resulting in low

sandstone/mudstone proportions. This is then capped by a high sandstone/mudstone interval with amalgamated, low sinuosity deposits.

The muddier isolated systems show a tendency for meandering, whereas coarser amalgamated systems show a tendency for braiding. This is consistent with models suggesting that sandstone/mudstone proportions are related to the river plan-form. The variations in the scale of channel-belts are also consistent with stacking patterns predicted in models relating sandstone/mudstone proportions to changes in the rate of aggradation, lateral migration, and avulsion frequency. These factors can be linked back to changes in accommodation, possibly indicating that it may be the determining factor.

Table of Contents

List of Figures

List of Tables

1. Introduction/Motivation

Understanding and predicting the architecture of fluvial deposits is very valuable, not only for research, but also for hydrocarbon exploration. Some of the biggest oil and gas producing fields have major fluvial reservoir components, such as Prudhoe Bay field in Alaska, Minas field in Sumatra, and Gippsland and Gorgon fields in Australia (Tye et al., 1999; Davies et al., 1991). This draws a special interest regarding the geometry, proportion, and spatial distribution of fluvial deposits, as these may influence the overall volume and connectivity of reservoirs, making them important elements in reservoir analysis (Davies et al., 1991; Gouw, 2007; Donselaar and Overeem, 2008). Predicting the architecture or organization of fluvial deposits, however, can be difficult. This is due to the complexity and variability of fluvial systems as a response to changes in discharge, slope, sediment grain size and load, and channel margin composition and strength (Bridge, 2006; Gibling, 2006; Ethridge, 2011). Nevertheless, several studies have attempted to address the architecture using qualitative models, proposing different controls on the resulting sandstone/mudstone proportions.

Earlier studies suggest that the sandstone/mudstone proportion (proportion of channel vs. floodplain deposits), is a function of the river plan-form, where the lack of muddy accreting deposits within high sandstone/mudstone proportions are indicative of braided systems (Friend, 1983). On the other hand, studies such as Bristow and Best (1993), suggest that the proportion of channel vs. floodplain deposits is not related to the river plan-form, but instead determined by changes in the rate of aggradation, lateral migration, and avulsion frequency, where low rates in aggradation and avulsion frequency and high rates in lateral migration result in high sandstone/mudstone proportions. The difference in opinion suggests that there is still some debate with regards to the actual control of sandstone/mudstone proportions in alluvial systems.

Although there has been a focus on the internal architecture of fluvial deposits, the external geometry is commonly used for subsurface analogues (Gibling, 2006). Since the earliest classification of sand body dimensions by Rich (1923), the focus has been on the relationship between the width (W) and thickness (T) of fluvial deposits (i.e. W/T ratio). Several W/T ratio values have been proposed in an attempt to characterize and define fluvial deposits (e.g. Krynine, 1948; Blakey and Gubitosa, 1984; Nadon, 1994). One of the most accepted division was introduced by Friend et al. (1979) and Friend (1983), wherein a W/T ratio value of 15 is used to separate ribbon-form (<15) from sheet-form channel bodies (>15). Gibling (2006) proposed a classification based on the dimensions of fluvial deposits, in which the width to thickness ratios are used to determine the style of a fluvial system (braided/low sinuosity, meandering, or distributive). This classification can be used to gain an understanding in regards to the type of fluvial system and its environment, especially when the internal architecture of fluvial deposits cannot be documented.

In this study, we describe and compare an ancient example of an amalgamated, high sandstone/mudstone proportion, channel-belt to underlying isolated, low sandstone/mudstone proportion, channel-belts within the Cretaceous Ferron Sandstone Member of the Mancos Shale Formation in south central Utah. The outcrop exposures along Sweetwater Wash provide an excellent opportunity to document the dimensions of several fluvial channel-belt deposits. This study attempts to determine fluvial style and depositional setting of the fluvial deposits by comparing documented channel-belt dimension to the dimensions of channel-belts in the literature (e.g. Gibling, 2006; Li and Bhattacharya, in review). Using the cross section (constructed from 25 vertical measured sections), bedding diagrams, paleocurrent measurements, and channel-belt dimensions, as well as lateral and vertical facies variations, we test the validity and applicability of fluvial and sequence stratigraphic models (e.g. Friend, 1983; Bristow and Best, 1993; Shanley and McCabe, 1993; Wright and Marriott, 1993; and Miall, 1996). Lastly, we attempt to determine possible systematic changes in channel-belt dimensions in order to relate the fluvial deposits to positioning within a sequence.

This detailed outcrop study may be used to better understand the organization of ancient fluvial deposits, which ultimately, may help refine existing fluvial reservoir models, especially in their application to the oil and gas industry.

2. Geologic Setting

The Ferron Sandstone Member of the Mancos Shale formation is middle Turonian to late Santonian in age, and was deposited as a series of fluvial deltaic complexes that prograded into the Cretaceous Western Interior Seaway. This was a shallow sea with faunal assemblages indicating a water depth of 250m to 300m (Kauffman, 1984) that was approximately 1600km wide, extending from the Gulf of Mexico to the present day Arctic Ocean, a distance of around 4800km (Kauffman, 1984).

The Ferron Sandstone formed as a result of sediment derived from continued thrusting of the Sevier orogenic belt to the west, and subsidence of the Cordilleran foreland basin (DeCelles and Giles, 1996; Ryer and Anderson, 2004), where sediment was being shed and deposited along the western margin of the seaway (Fig 2.1), resulting in eastward thinning clastic wedges.

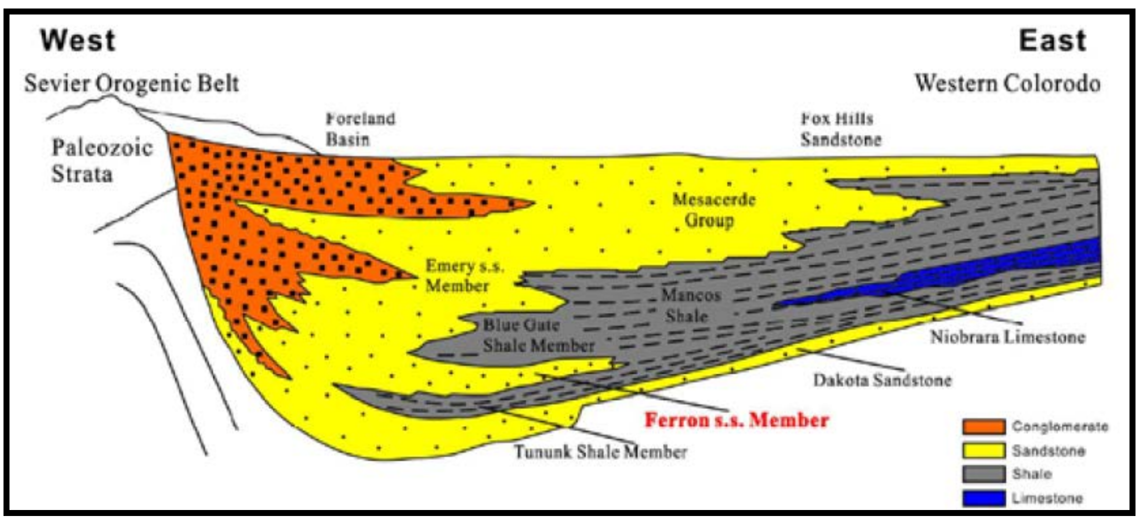

Figure 2.1 Cross section demonstrating the regional stratigraphy of the research area, where the Ferron Sandstone Member (in yellow) was deposited into the Cordillera foreland basin. It pinches out towards the east and is bounded by the Tununk Shale (below) and the Blue Gate Shale (above). (Armstrong, 1968)

Three fluvial deltaic complexes (Fig. 2.2) were identified, the Vernal, Last

Chance, and Notom Deltas, all of which prograded in a northeast to east direction (Gardner, 1995; Garrison and van den Bergh, 2004; Li et al., 2010; Zhu et al., 2012).

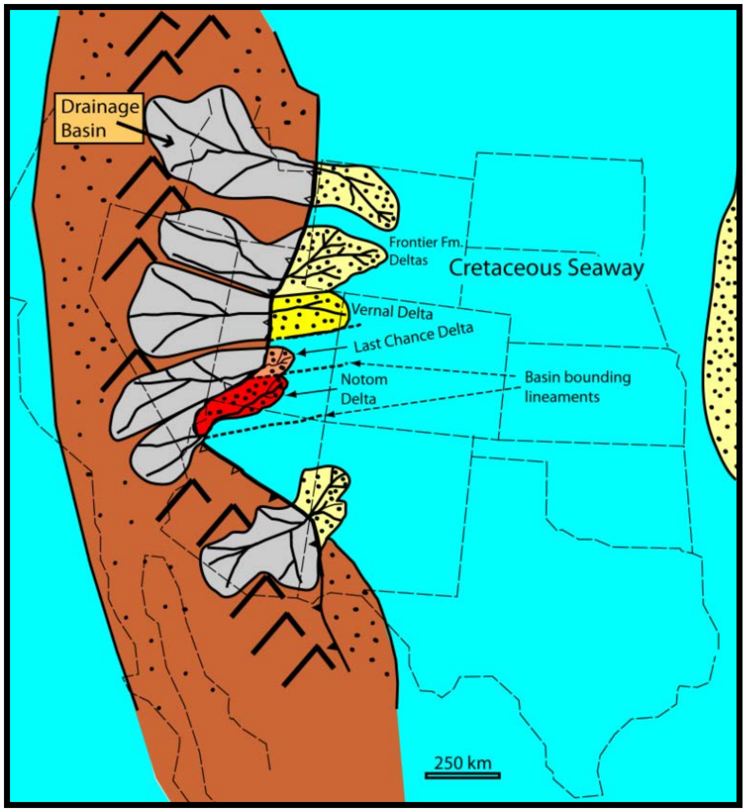

Figure 2.2 Paleogeographic map demonstrates a series of fluvial deltaic complexes prograding into the Cretaceous Western Interior Seaway. The Notom Delta (highlighted in red) was 1 of 3 eastward thinning clastic wedges of the Ferron Sandstone Member. (Bhattacharya and Tye, 2004)

The southernmost lobe, the Notom Delta complex, (Fig. 2.2) first prograded into the Henry Mountains Basin (91.25-90.7 Ma) prior to a regional river avulsion towards the north, leading to the formation of the Last Chance Delta in the Castle Valley area (Gardner, 1995; Garrison and van den Bergh, 2004). Zhu et al. (2012) determined that the entire Ferron Notom Delta was deposited in about 620,000 years. The Ferron Sandstone sits above the Tununk Shale Member, and below the Bluegate Shale Member (Garrison & van den Bergh, 2004). Peterson and Ryder (1975) divided the Ferron into lower shallow marine deposits and upper predominantly fluvial units. A regional sequence stratigraphic framework of the Ferron Notom Delta was constructed by Zhu et al. (2012) and Li et al. (2010), in which they identified 43 parasequences, 18 parasequence sets, and 6 sequences. This study focuses on the fluvial deposits within the youngest sequence 1 (Fig. 2.3 & 2.4).

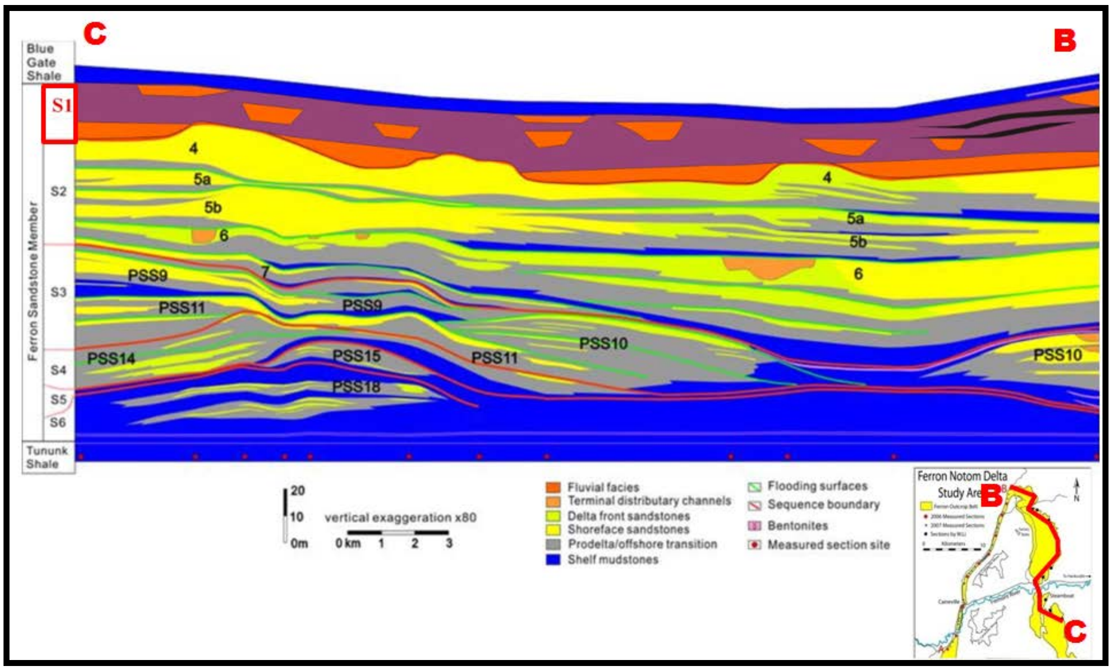

Figure 2.3 Strike view section dividing the Ferron Notom Delta into 43 parasequences, 18 parasequence sets, and 6 sequences. This study focuses on the fluvial facies within sequence 1. (Zhu et al., 2012, after Li et al., 2010)

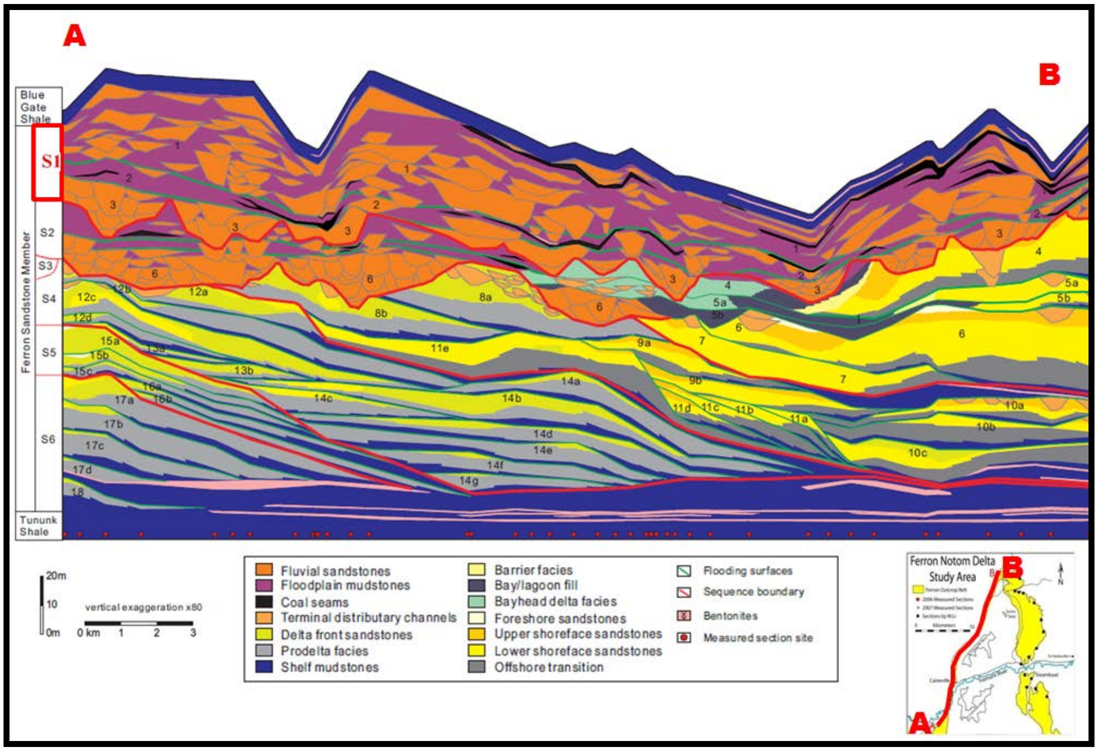

Figure 2.4 Dip view section dividing the Ferron Notom Delta into 43 parasequences, 18 parasequence sets, and 6 sequences. This study focuses on the fluvial facies within sequence 1. (Zhu et al., 2012, after Li et al., 2010)

3. Study Area/Previous Work

The study area is located south of U.S. Highway 24 and the Freemont River, between the towns of Hanksville and Caineville, near Sweetwater Creek in south-central Utah, U.S.A. (Fig 3.1). The exposures consist of several near vertical cliffs, ranging from 10m to 15m in height, that expose numerous fluvial channel-belts along Sweetwater Wash. This allows the comparison of a coarser grained amalgamated channel-belt to finer grained isolated channel-belts, which are encased in floodplain mudstones.

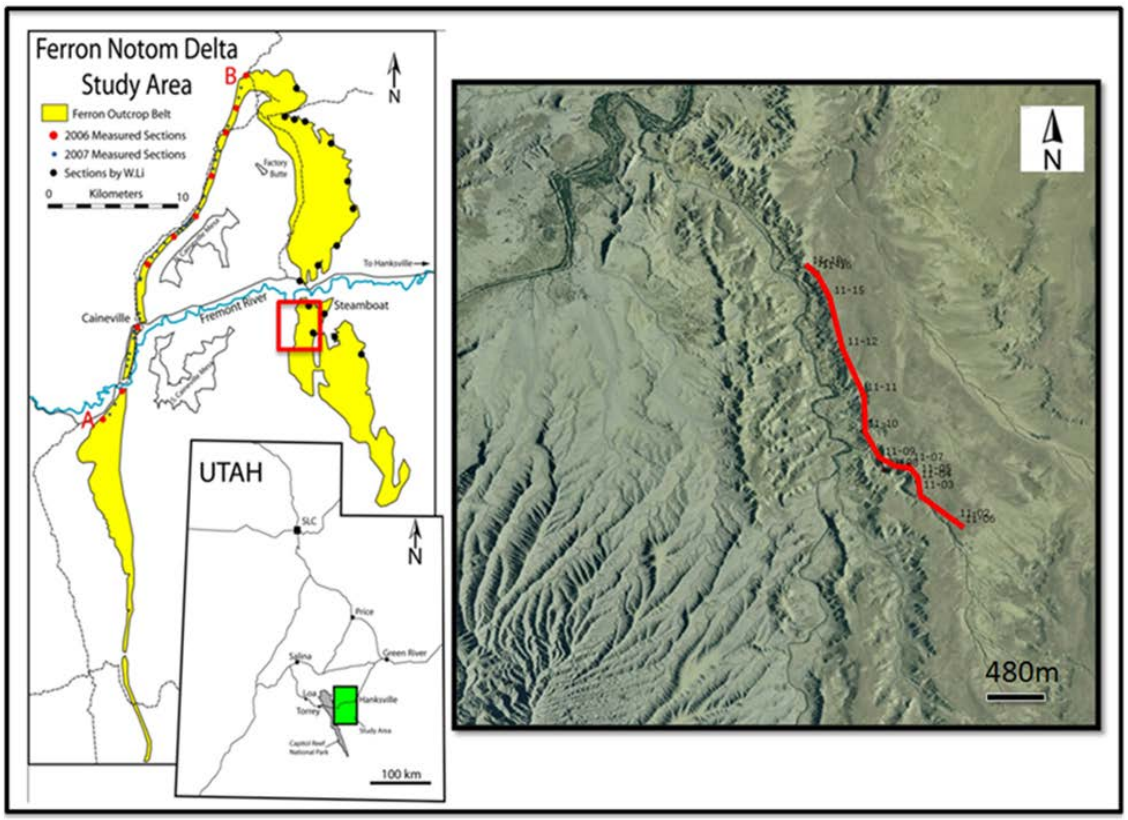

Figure 3.1 Diagram to the left is a map showing the outcrop exposure of the Ferron Sandstone in South Central Utah between the towns of Hanksville and Caineville. Diagram to the right is an aerial photo of the research area showing the locations of the vertical measured sections.

Within sequence 1, Li et al. (2010) recognized two valley fills, in which a vertical change in facies and fluvial style was documented associated with changes in water discharge, sediment load, and slope. In the older valley 2, the fluvial style appears to have always been meandering, in contrast to the younger valley 1, which demonstrates a change from braided at the base to single thread meandering then back to a braided system. The sandstone at the base of the valley is interpreted as lowstand fluvial deposits, being highly amalgamated and exhibiting a high sandstone/mudstone ratio. The highstand fluvial deposits were observed to have low sandstone/mudstone ratio and the presence of isolated and non-amalgamated channels and channel-belts, as well as an abundance of finer grain sediment associated with floodplain deposits (Li et al., 2010). This study focuses on documenting the fluvial deposits above valley 1 within sequence 1, the isolated channel-belts and the overlying amalgamated “sheet-like” channel-belt, interpreted as the highstand systems tract by Li et al. (2010).

4. Methodology

Data for the 25 vertical measured sections were collected by trenching and using a hand lens, rock hammer, grain size card, Brunton compass, tape measure, Jacob staff, and GPS. The measured sections recorded variations in grain size, sedimentary structures, paleocurrent direction, and preserved cross-set thickness. Measured sections were scanned, digitized, and correlated to create an oblique to mean paleocurrent direction cross section, using the overlying transgressive Bluegate Shale Member as a datum to hang the measured sections from. The cross section (Fig. 4.1) demonstrates the stacking of different channel-belts throughout Sweetwater Wash. In total, three different channel-belt groups are identified. A lower section that is amalgamated (CHB. C), a middle section consisting of isolated channel-belts (CHB. B), and an upper section that also consists of an amalgamated channel-belt (CHB. A). This study focuses on the upper amalgamated channel-belt (CHB. A) and the middle isolated channel-belts (CHB. B).

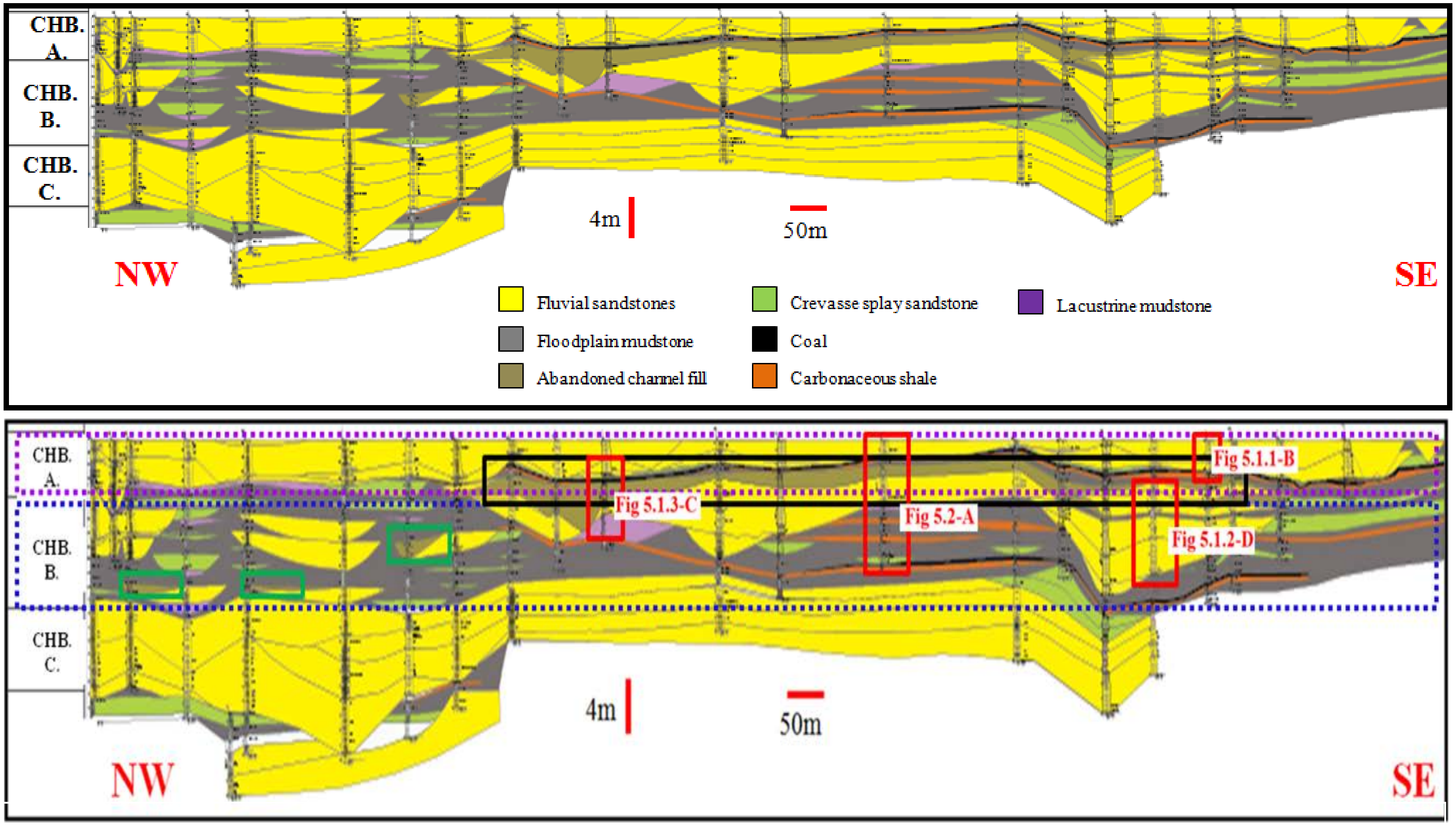

Figure 4.1 Northwest to Southeast cross section created from 25 vertical measured sections, where the Bluegate Shale Member was used as the datum to hang the measured sections from. In the lower cross section the top amalgamated channel-belt (CHB. A.) is outlined with a purple dashed polygon. The isolated channel-belts (CHB. B.) are outlined with a blue dashed polygon. The red polygons represent vertical measured sections demonstrating different facies, discussed later in the paper. The green polygons represent the very fine-grain sandstone to siltstone facies seen at the margins of channel-belts, discussed later in the paper. The black polygon represents the very fine-grain sandstone to siltstone facies draping an isolated channel-belt a distance of approximately 1100 meters, discussed later in the paper.

Highly detailed photos were taken of the outcrop using a gigapan and DSLR cameras. The photos were then merged together using Adobe Photoshop and Gigapan Software to create photomosaics. Measured sections were then superimposed on the photomosaics, and correlated to create bedding diagrams documenting the internal architecture of the fluvial deposits. Miall's (1992) classification of bounding surfaces was used to identify and number the different order surfaces associated with architectural elements. In the bedding diagrams, zero order surfaces bound features on the lamina scale, 1st order surfaces represent set boundaries, 2nd order surfaces bound co-sets, 3rd order surfaces bound individual flood packages or deposits (sets of co-sets), 4th order surfaces represent bar tops, 5th order surfaces represent the erosional base of a channel, and 6th order surfaces represent the base of a channel-belt.

Paleocurrent measurements were collected, analyzed, and compared to bedding diagrams to determine the direction of paleoflow in relation to bar accretion surfaces. This allows river plan-form (e.g. meandering vs. braided) to be determined.

Channel-belt thickness was obtained from the vertical measured sections and channel-belt width was obtained by taking GPS readings at their respective margins, where exposed. Channel-belt dimensions obtained from the GPS readings were then verified with values obtained from the cross section. Channel-belt widths had to be corrected due to the cross section being oblique to mean paleocurrent direction. Corrections were done by obtaining numerous paleocurrent measurements to determine mean paleoflow direction of the system, obtaining the outcrop orientation, as well as the apparent channel-belt width. By applying basic trigonometric principles to this information, interpreted actual channel-belt width were calculated.

5. Facies Analysis

We have identified 2 major facies successions, fluvial and floodplain succession, in this study. These are subdivided into 9 individual facies based on lithology, sedimentary structures, and biogenic features, as demonstrated in Table 1.

Major Facies Succession	Facies	Lithology	Sedimentary Structures	Biogenic Features
Fluvial Succession	F1	Coarse- to medium-grained pebbly sandstone with mud clasts	Dune-scale cross beds	Teredolites burrows
	F2	Medium- to very fine-grained sandstone with mud clasts and pebble lags	Dune-scale cross beds, planar bedding, and ripple cross-laminations	Root traces and plant material
	F3	Very fine-grain sandstone to siltstone	Ripple cross laminations	Root traces, plant material, and coaly organic material
Floodplain Succession	FP1	Mudstone	Horizontal laminations with some slickensides	Small amounts of root traces and coaly organic material
	FP2	Silty to fine-grained sandstone, at times interbedded with mudstone	Ripple cross laminations and some dune-scale cross bedding.	Root traces and plant material
	FP3	Coal	---	---
	FP4	Mudstone to siltstone	Abundant slickensides and soil mottles	Abundant plant and coaly organic material, evidence of root traces
	FP5	Mudstone to siltstone	Slickensides and soil mottles	Variable amount of root traces and very minimal coaly organic material
	FP6	Mudstone to very fine-grained sandstone interbedded with mudstone	Horizontal and ripple cross laminations with some slickensides	Plant material and evidence of coaly organic material

Table 1. Table summarizing facies documented within the study area.

5.1 Fluvial Succession

The fluvial succession is subdivided into three facies: F1, coarse- to medium-grained sandstone; F2, medium- to very fine-grained sandstone; and F3, very fine-grained sandstone to siltstone.

5.1.1 F1, Coarse- to medium-grained sandstone

Description:

The coarse- to medium-grained sandstone facies is associated with the upper amalgamated channel-belt (Fig 4.1). This facies ranges in thickness from 1.2m to 3.5m, with an average thickness of 2.5m. A minimum apparent width of 4.4km (minimum true (corrected) width of ~2.8km) was documented for this sand body, representing the distance from the only exposed channel-belt margin (exposed at the southern end of the cross section) to the northern end of Sweetwater Wash (extending past the north end of the cross section). The exposed surface of this sandstone facies does not show much variation, making it difficult to document internal bedding or architecture. There is, however, a pebble lag and an abrupt change in grain size, which allows scour surfaces associated with individual storeys to be recognized in some locations. The sandstone body is made up of two to three individual storeys, ranging in thickness from 0.4m to 2.5m (Fig. 5.1.1-A&B). Each storey demonstrates a fining upward from coarse-grained dune-scale cross-stratified pebbly sandstone to medium-grained dune-scale cross-stratified sandstone (Fig. 5.1.1-B&C). This sandstone facies erosionally sits on a coal unit, approximately 20cm thick (Fig. 5.1.1-B&D), all the way to the southern end of the cross section, a distance of approximately 1300m. Towards the northern end of the cross section, however, the sandstone erosionally sits on finer floodplain facies (Fig. 5.1.1-E), a distance of approximately 600m, with evidence of preserved mud clast at these locations. Paleocurrent measurements for this facies do not show much variation, suggesting flow direction was predominantly northeast.

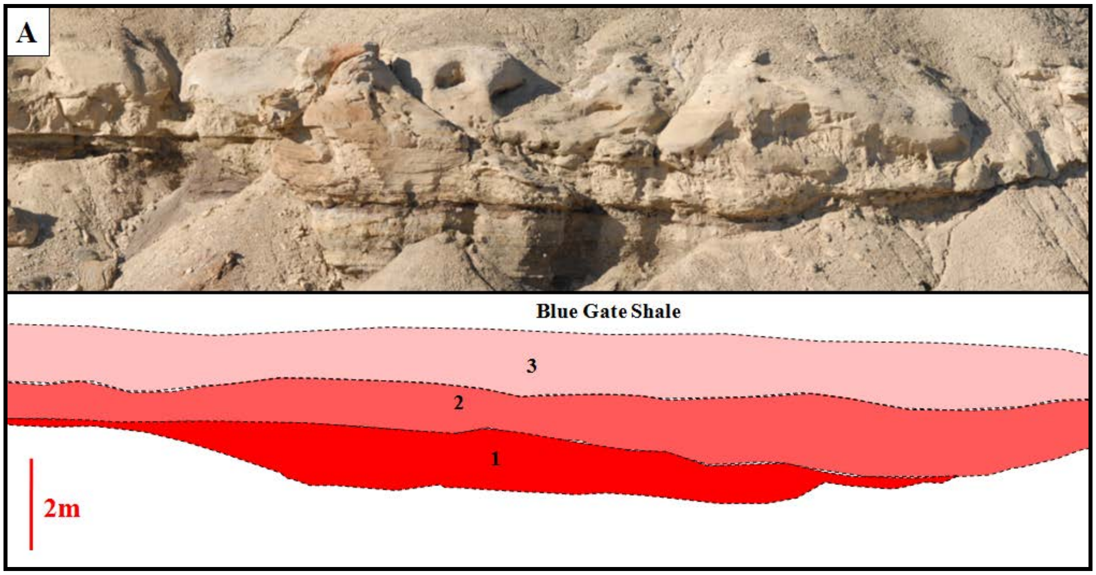

Figure 5.1.1-A. Photo of the outcrop (above) and bedding diagram (below) demonstrating the multi-storey (3 storey) nature of the sandstone body at the northern end of the cross section represented by the different colored polygons. The 1st storey demonstrates an average thickness of ~1m, the 2nd storey demonstrates an average thickness of ~ 0.8m, and the 3rd storey demonstrates an average thickness of ~1.3m.

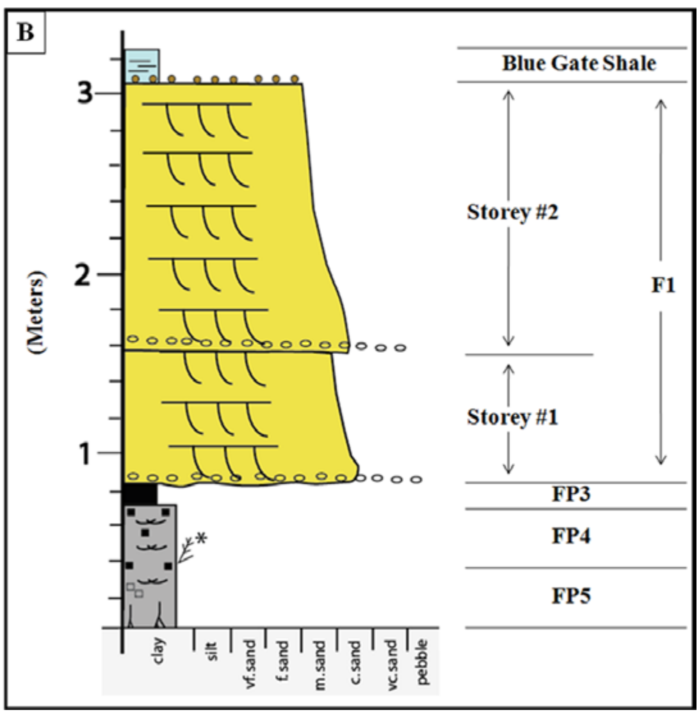

Figure 5.1.1-B. Typical section demonstrating the multistorey nature of the fining upwards coarse- to medium-grained dune-scale cross-stratified pebbly sandstone erosionally sitting above a 20 cm thick coal unit. Refer back to figure 4.1 for location on the cross section.

Figure 5.1.1-C. Dune-scale cross-bedded coarse- to medium-grained pebbly sandstone.

Figure 5.1.1-D. Coarse- to medium-grained pebbly sandstone erosionally sitting above a 20cm thick coal unit towards the southern end of the cross section.

Figure 5.1.1-E. Coarse- to medium-grained pebbly sandstone erosionally sitting above a finer floodplain facies towards the northern end of the cross section.

Interpretation:

The undulating scour base/surface and fining upward are indicative of waning flow in a fluvial system. The pebble lag suggests that the system experienced episodes of increased flow rates (Bridge, 2006). The dominance of dune-scale cross-stratified sandstone suggest that if smaller scale ripple bed-forms were ever deposited, they were eroded away by the following flood event, preventing their preservation in the rock record. The increase in the amount of preserved mud clasts in areas where the sandstone was not erosionally sitting above the coal unit, suggests that the system was now eroding into finer grained floodplain sediment. The low variation in grain size is believed to be the main cause behind the lack of internal architecture, suggesting that this was predominantly a high energy system.

The coarser grain size of the channel fill deposit, lack of laterally accreting deposits, low variations of paleocurrent measurements, and "sheet-like" geometry suggest that this was a low sinuosity, multi-channel possibly braided system (Bridge, 2006; Shanley and McCabe, 1993).

5.1.2 F2, Medium- to very fine-grained sandstone

Description:

The medium- to very fine-grained sandstone facies is seen associated with the isolated channel-belts (Fig 4.1), and are far less extensive (Fig. 5.1.2-A&B). There are a total of eleven isolated sandstone bodies identified within the study area, demonstrating a variety of dimensions. They range in thickness from 1.1m to 5m, and from 40m to 245m in true (corrected) width. The isolated sandstone facies are completely encased within finer grained deposits (Fig. 5.1.2-C). Basal scour surfaces, in places, show mud clasts, pebble lags, or abrupt changes in grain size, suggesting a multi-storey nature (Fig. 5.1.2-D). The 2 isolated multi-storey sandstone bodies consist of two to three individual storeys that range in thickness from 0.8m to 2.4m (Fig. 5.1.2-D&E), whereas the remaining 9 isolated single storey sandstone bodies range from 1.1m to 2m thick. Individual storeys show a fining upward, from medium-grained sandstone to very fine-grained sandstone. Sedimentary structures associated with this facies are dune-scale cross-beds (Fig. 5.1.2-D&F) and planar bedding (Fig. 5.1.2-D&G). Near the tops and margins of some of these sandstones are ripple cross-laminations (Fig. 5.1.2-D&H) with evidence of plant material and root traces. Paleocurrent direction for this facies varies depending on location and channel storey. For the most part, paleocurrent direction is towards the northeast, however, variations in measurements suggest a range from northwest to east. The documented internal architecture captures several sandstone bodies with large-scale accreting beds that appear to dip perpendicular to the paleocurrent direction (be discussed later in the paper).

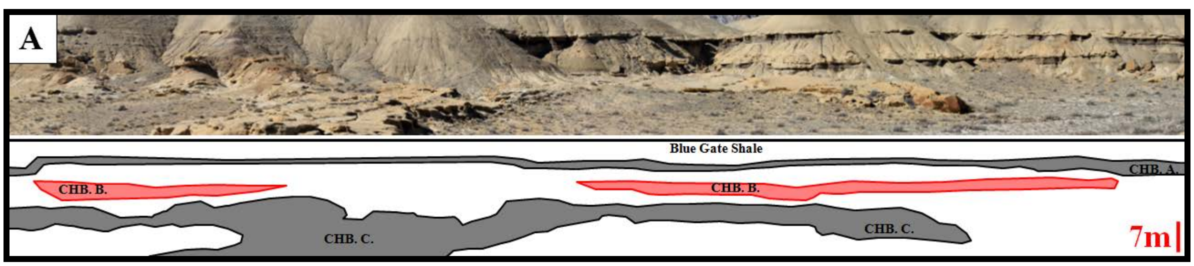

Figure 5.1.2-A. Photo of the outcrop (above) and bedding diagram (below), demonstrating the isolated medium- to very fine-grained sandstone bodies (red polygons) exposed at the northern end of the cross section, all of which have different dimensions (width and thickness).

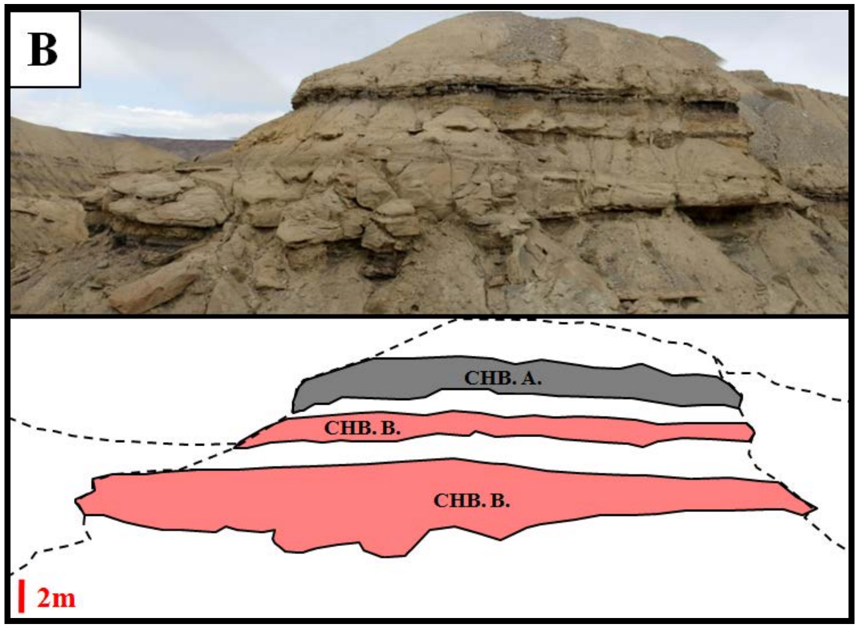

Figure 5.1.2-B. Photo of the outcrop (above) and bedding diagram (below), demonstrating the isolated medium- to very fine-grained sandstone bodies (red polygons) exposed towards the southern end of the cross section, all of which have different dimensions (width and thickness).

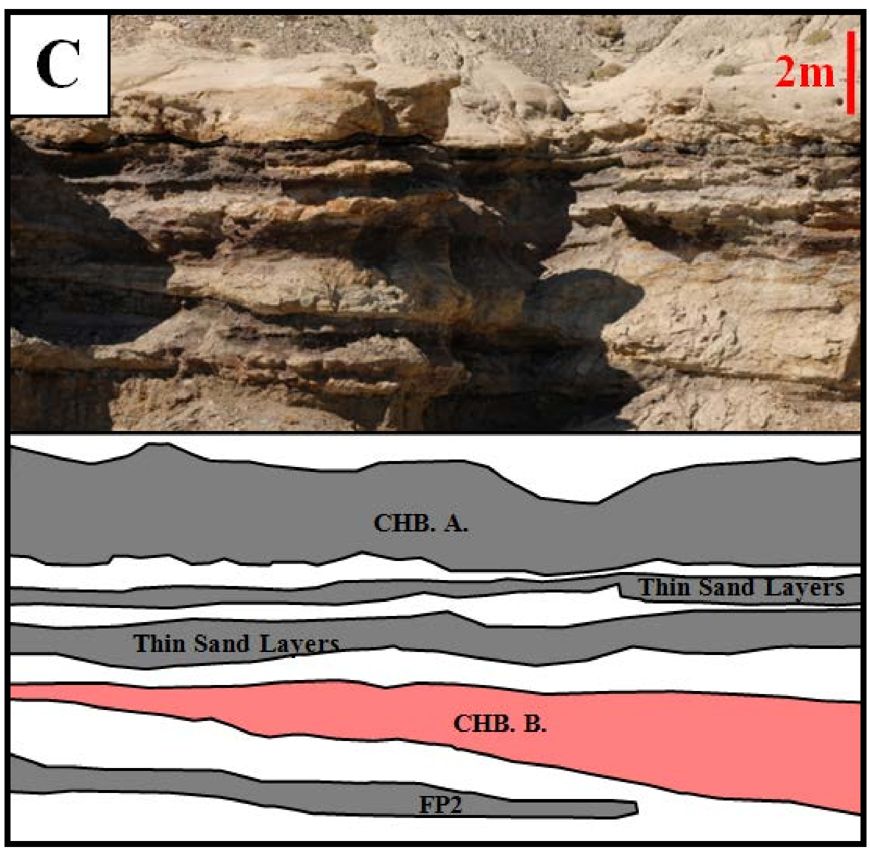

Figure 5.1.2-C. Isolated medium- to very fine-grained sandstone facies (red polygon) encased within finer grain sediment (white region).

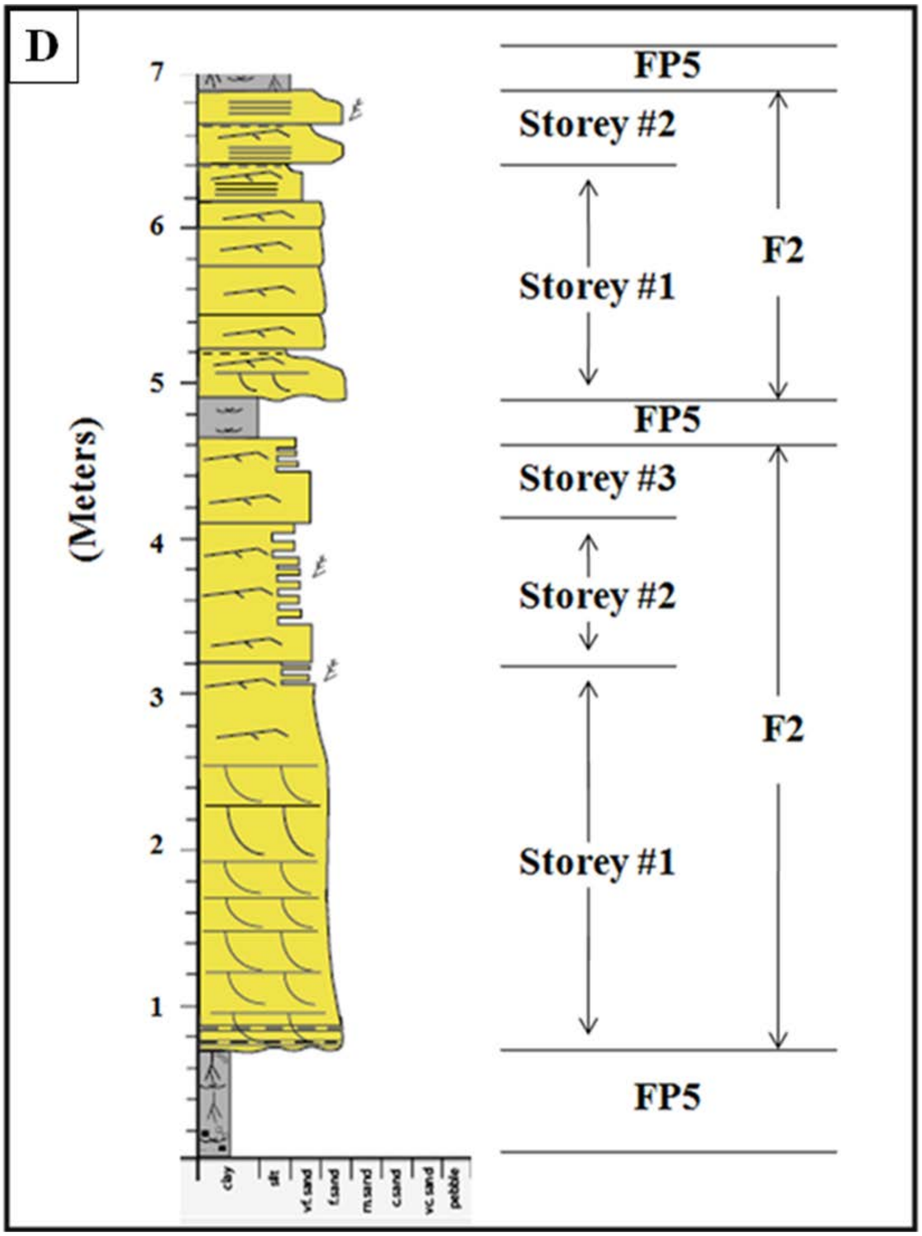

Figure 5.1.2-D. Typical section demonstrating the multistorey nature of the fining upwards of the medium- to very fine-grained sandstone, erosionally sitting above finer grain sediment. Sedimentary structures associated with this facies are dune-scale cross beds, planar beds, and ripple cross laminations. Refer back to figure 4.1 for location on the cross section.

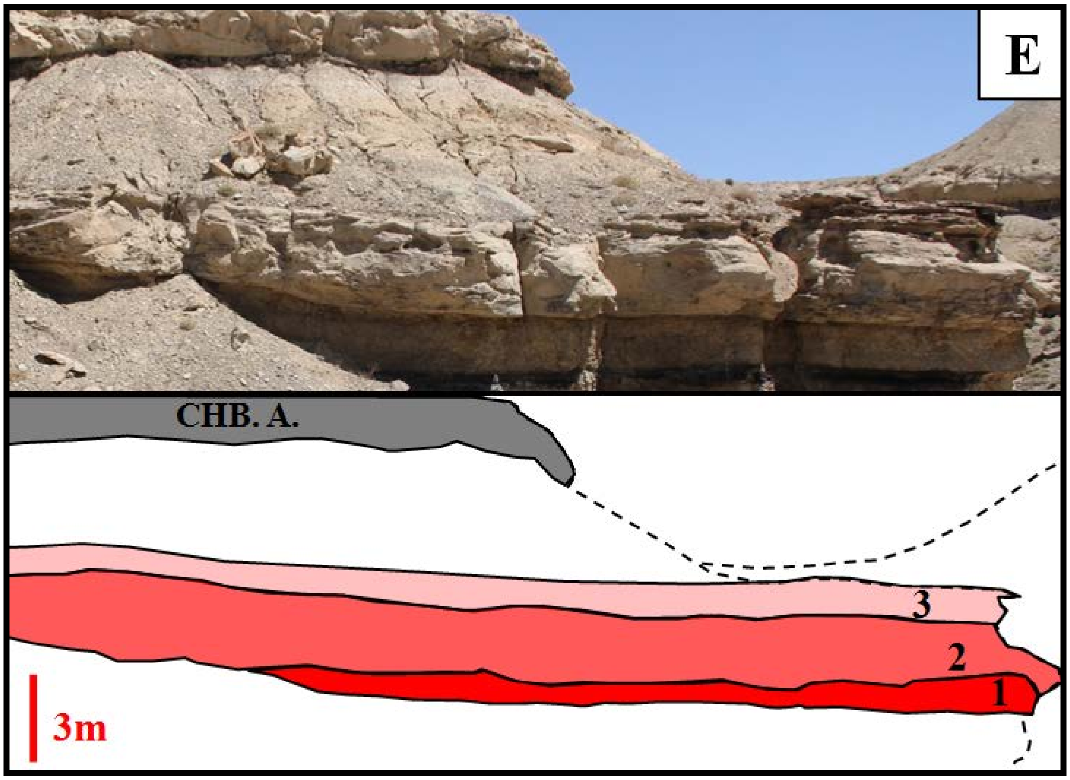

Figure 5.1.2-E. Photo of the outcrop (above)and bedding diagram (below) demonstrating the multi-storey (3 storeys) nature of the medium- to very fine-grained isolated sandstone body (CHB. B), represented by the different colored polygons. The 1st storey is 0.7m thick, the 2nd storey was 1.8m thick, and the 3rd storey was 2.3m thick.

Figure 5.1.2-F. Dune-scale cross beds associated with the medium- to very fine-grained sandstone facies.

Figure 5.1.2-G. Planar bedding associated with the medium- to very fine-grained sandstone facies.

Figure 5.1.2-H. Ripple cross laminations towards the top of the medium- to very fine-grained sandstone facies.

Interpretation:

The much less extensive geometry of the sandstone deposit, greater proportion of finer grained sediment adjacent to the sandstone deposit, greater variations in paleocurrent measurements, and the internal geometry demonstrating laterally accreting deposits, suggest that these were moderate to highly sinuous fluvial systems (Bridge, 2006). The mud clasts, pebble lags, and plant material preserved within the sandstones, along with the preservation of laterally accreting deposits, which accrete at high angles to paleocurrent direction, suggest that these are point bars associated with meandering systems that laterally migrated and eroded into vegetated, finer grained floodplains (Shanley and McCabe, 1993).

The fining upwards, grading from dune-scale cross-bedded to ripple cross-laminated to even massive sandstones, can be attributed to a decrease or waning of the flow and a decrease in velocity and grain size towards the top of the point bar, favoring the preservation of smaller scale bed-form features. The root traces and plant material found towards the top and margins of the sandstones bodies infer that the upper portion of the point bars did not experience much activity and erosion, allowing vegetation to become established (Shanley and McCabe, 1993).

5.1.3 F3, Very fine-grain sandstone to siltstone

Description:

The very fine-grained sandstone to siltstone facies is seen draping the medium- to very fine-grained isolated sandstone facies (Fig. 5.1.3-A). It sometimes demonstrates a U-shaped channel form geometry (Fig. 5.1.3-B), where the sediment filling the channel form is generally finer grain than the adjacent bar deposits. In general, this facies occurs at the margins of a channel-belt and are significantly narrower than the sandstone deposit, being less than 50m wide on average (refer to Fig. 4.1). However, in one case, this facies is much more extensive and is seen on the cross section draping an upper isolated channel-belt a distance of approximately 1100m (apparent (uncorrected) width) (refer to Fig. 4.1). The thickness of this facies ranges from 0.4m up to approximately 2m, averaging a thickness of about 1m. This facies generally shows a fining upward from very fine-grained sandstone to siltstone (Fig. 5.1.3-C) with evidence of root traces as well as plant and coaly organic material (Fig. 5.1.3-C&D). Sedimentary structures associated with this facies are ripple cross laminations. In some locations, thin sandstone beds or layers are seen within the facies (Fig. 5.1.3-A&E).

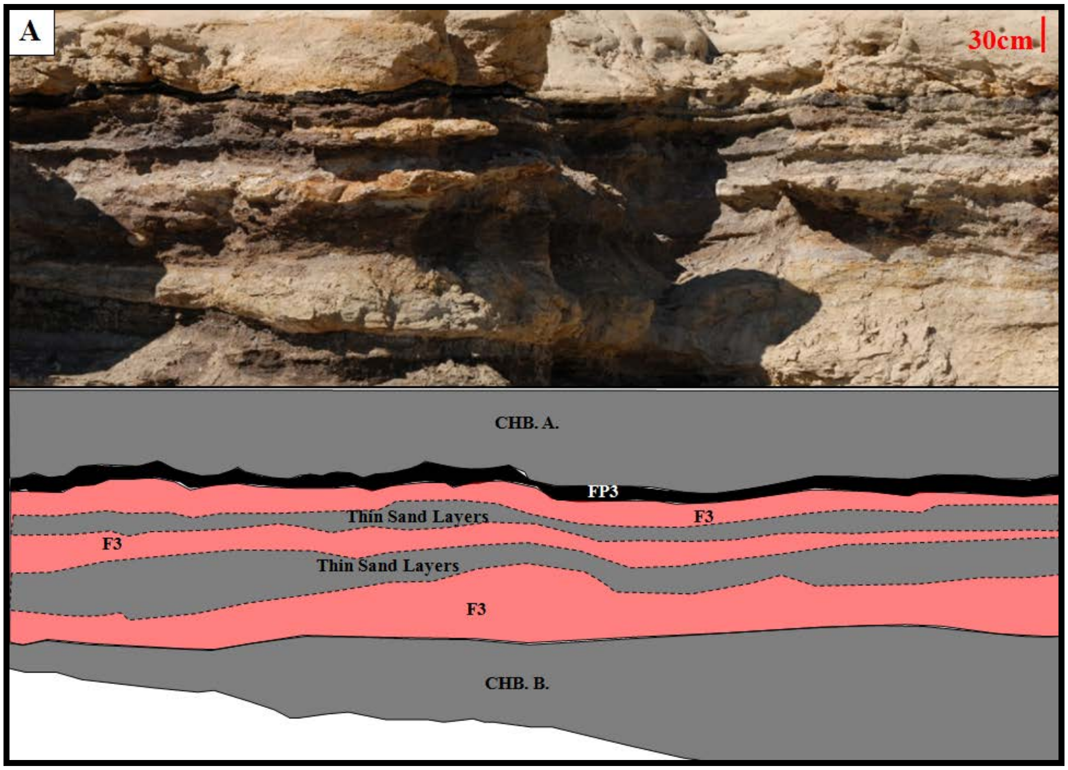

Figure 5.1.3-A. Very fine-grained sandstone to siltstone facies (F3, red polygons) draping the isolated medium- to very fine-grained sandstone body (CHB. B). Thin sandstone beds or layers are seen within the facies in some locations.

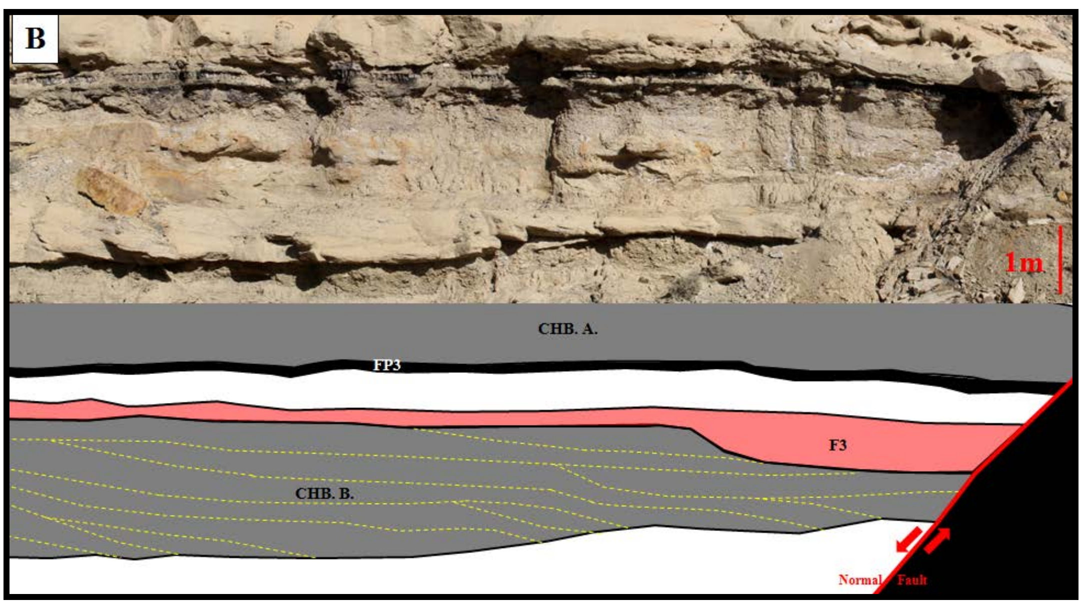

Figure 5.1.3-B. Very fine-grained sandstone to siltstone facies (F3, red polygon) filling the U-shaped channel form geometry. Sediments filling the channel form are muddier than adjacent bar deposits.

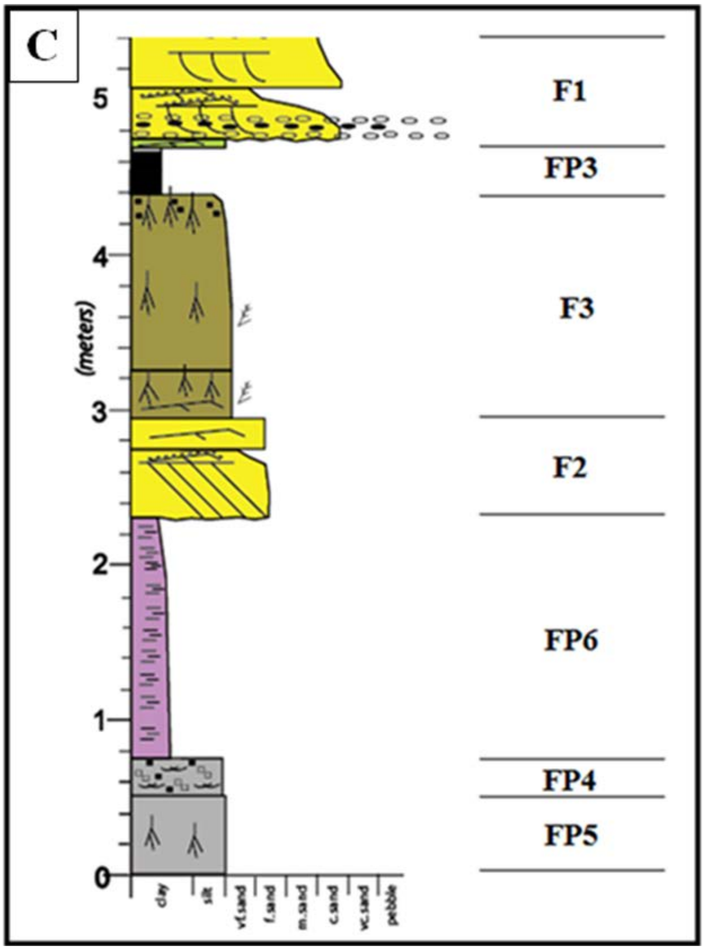

Figure 5.1.3-C. Typical section demonstrating the very fine-grained sandstone to siltstone facies. Sedimentary structures associated with this facies are ripple cross laminations with evidence of root traces as well as plant and coaly organic material. Refer back to figure 4.1 for location on the cross section.

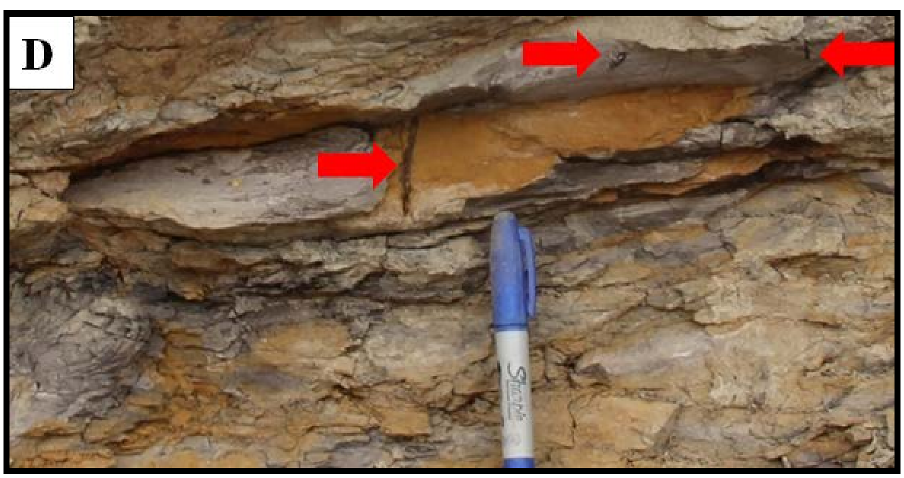

Figure 5.1.3-D. Arrows point to root traces and plant material within the very fine-grained sandstone to siltstone facies.

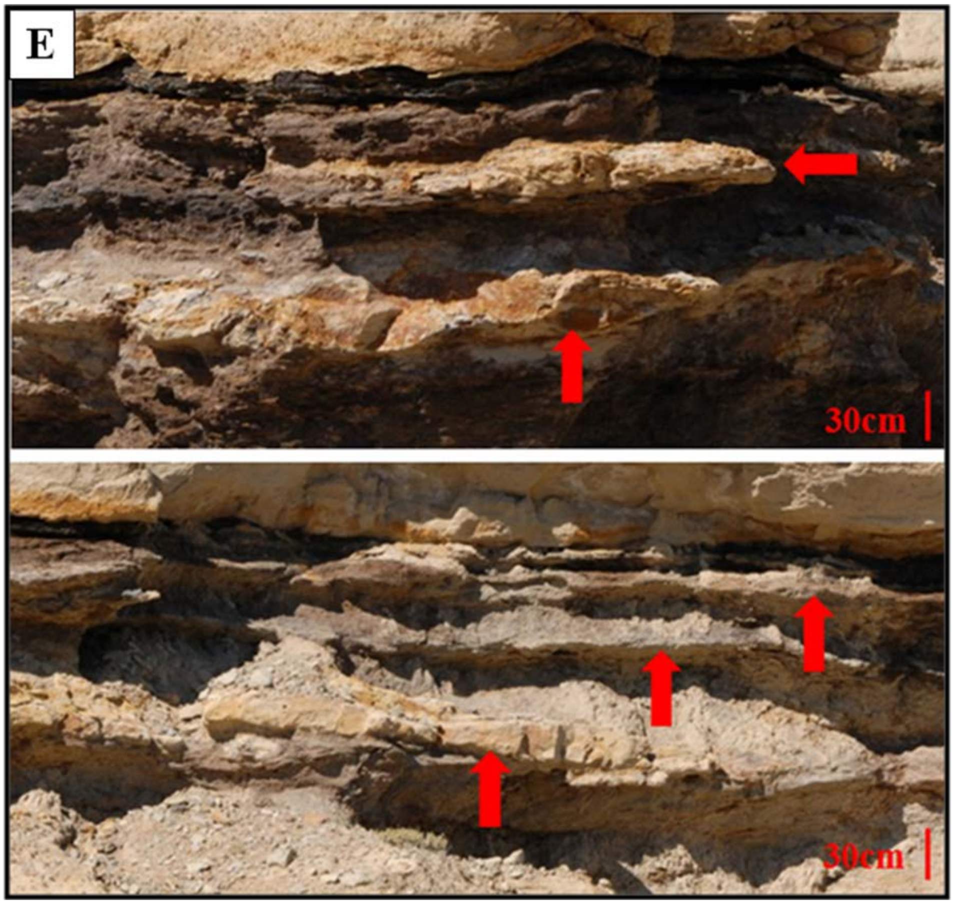

Figure 5.1.3-E. Arrows point to thin sandstone layers within the very fine-grained sandstone to siltstone facies, only present in some locations.

Interpretation:

The very fine-grain to silt-size sediment, root traces, plant and coaly organic material, along with the ripple laminations, suggest that this was not a high energy environment, allowing vegetation to become established. The U-shaped geometry, along with its lateral extent (draping the medium- to very fine-grained isolated sandstone), suggest that this facies could be a combination of a muddier upper channel fill (trailing the underlying migration of the sandier point bar) and abandoned channel fill deposit. Depending on the orientation or obliquity of the upper channel/abandoned channel fill to the outcrop, the lateral extent of this facies (i.e. width) may be overestimated.

The thin sandstone layers found within this facies indicate an influx of coarser sediment from time to time (during flood events), possibly related to a gradual rather than abrupt abandonment.

5.2 Floodplain Succession

The floodplain succession is subdivided into six facies: FP1, mudstone; FP2, siltstone to fine-grained sandstone; FP3, coals; FP4, carbonaceous shale; FP5, mudstone to siltstone; and FP6, mudstone to very fine-grained sandstone. Although it appears that the floodplain/mudstone successions are relatively continuous, individual facies elements are eroded into by channels or interfinger with other floodplain facies. Therefore, the lateral extent is based on analysis of continuous, uninterrupted facies. The floodplain succession is the primary focus of Oyebode Famubode (Ph.D. candidate), therefore only a brief basic description and interpretation will be given here (Table 1).

5.2.1 FP1, Mudstone

Description:

This facies consists of a mudstone lithology extending laterally on the order of hundreds of meters with a thickness on the order of meters. It is horizontally laminated with very small amounts of root traces, coaly organic material, and slickensides (Refer to Fig. 4.1).

Interpretation:

The lithology, horizontal laminations, minimal rooting, and coaly organic material, suggest that the energy and sedimentation of this environment was sufficient enough to prevent the establishment of abundant vegetation. The presence of slickensides suggest cycles of wet and dry periods. This mudstone facies is found below as well as separating some of the fluvial sandstone deposits, suggesting that these may be floodplain deposits.

5.2.2 FP2, Siltstone to fine -grained sandstone

Description:

This facies is made up of silty to fine-grained ripple cross-laminated to even dune-scale cross-bedded sandstone, which at times is interbedded with mudstone. The thickness of this facies ranges on the order of centimeters up to 1.5m, laterally extending tens to hundreds of meters. This facies has a blocky to fining upward profile and is found adjacent to fluvial sandstones, demonstrating a sheet or wedge-shape geometry that decreases in thickness (becoming thinner) with increasing distance away from the channel-belt margin. It contains evidence of root traces and plant material (Refer to Fig. 4.1 & Fig. 5.2-A).

Interpretation:

The lithology, root traces, and plant material suggest that this was a low energy depositional environment with not much erosion, allowing vegetation to become established. The wedge shape geometry and lateral relationship to fluvial sandstones suggest that these are crevasse splays found adjacent to once active channels.

5.2.3 FP3, Coals

Description:

This facies forms thin black beds or horizons, approximately 20cm thick, that extend for hundreds of meters up to 1300m. In total, there are 4 distinct horizons but only 2 are extensive, one sitting right beneath the uppermost amalgamated channel-belt (CHB.

A) for approximately 1300m, towards the southern end of the cross section (Fig 5.1.1-D), and the other is encased within finer floodplain sediment beneath isolated channel-belts (CHB. B) (Fig. 4.1 & Fig. 5.2-A).

Interpretation:

This facies represents coal seams created by the compaction of plant matter. The depositional environment is interpreted to have been associated with a swamp or marsh environment, where there is a great abundance of plant matter.

5.2.4 FP4, Carbonaceous shale

Description:

This facies is made up of mudstone to siltstone containing high amounts of plant material, coaly organic material, and slickensides (Fig. 5.2-A & B). There is also evidence of soil mottles and root traces. The thickness of this facies is on the order of centimeters, and the width is on the order of hundreds of meters (Refer to Fig. 4.1).

Interpretation:

The fine lithology, abundance of plant material, root traces, and slickensides (wet and dry periods) suggest that this was possibly a swamp or marsh environment, but with a higher degree of clastic input than FP3.

5.2.5 FP5, Mudstone to siltstone

Description:

This gray color mudstone to siltstone facies contains evidence of slickensides, soil mottles, variable amount of root traces, and very little to no coaly organic material (Fig. 5.2-A & C). Its thickness is on the order of centimeters to meters, and its width is on the order of hundreds of meters (refer back to Fig. 4.1).

Interpretation:

Paleosols are designated on the basis of extensive pedogenic alterations that disallow easy interpretation of the precursor lithology. However, they may initiate with all previously described facies. Even though the pedogenic degree of alteration is too extensive to interpret the original depositional environment, the gray color and root traces suggest that these are relatively immature paleosols, which may indicate relatively humid environments. These are further addressed in detail by Famubode (in prep), where paleosols are distinguished as unique facies.

5.2.6 FP6, Mudstone to very fine-grained sandstone

Description:

This facies is made up mudstone to very fine-grained sandstone interbedded with mudstone (Fig. 5.2-A). It is horizontally and ripple cross laminated, with a thickness on the order of centimeters up to 1.5 meters (Fig. 5.2-D), and a width on the order of tens of meters (Refer to Fig. 4.1). It contains plant material, as well as evidence of coaly organic material and slickensides. This facies commonly sits below fluvial or crevasse splay sandstones, and above finer grain sediment (paleosols).

Interpretation:

The fine lithology as well as the small scale cross laminations suggest that this was a low energy environment. The presence of plant material and coaly organic material suggest that this was possibly a swamp or lake environment. The poor development of slickensides may indicate that this was a wetter environment compared to the environments associated with the other FP facies. The presence of this facies beneath fluvial or crevasse splay sandstones could indicate that they were deposited within low areas or areas of depression within the floodplain. This facies is distinct from FP4 due to its lower carbonaceous composition.

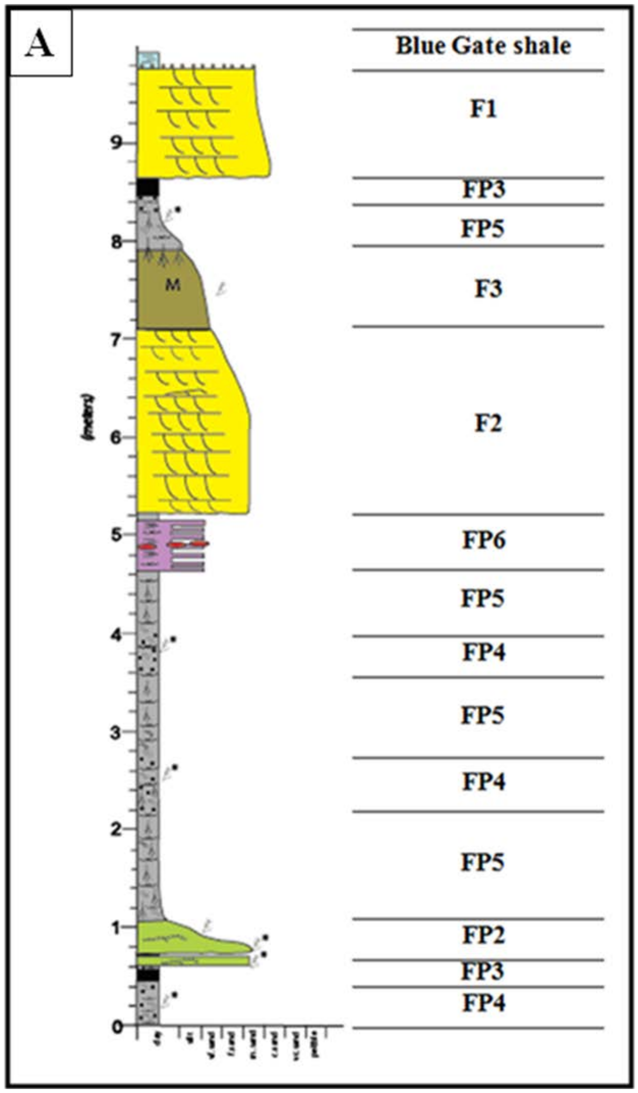

Figure 5.2-A Typical section demonstrating all of the facies associated with the floodplain succession. Refer back to figure 4.1 for location on the cross section.

Figure 5.2-B FP4, Mudstone to siltstone (carbonaceous shale) facies containing high amounts of plant and coaly organic material.

Figure 5.2-C FP5, Gray color mudstone to siltstone facies containing root traces.

Figure 5.2-D FP6, Mudstone to very fine-grained sandstone facies (making up the entire photo). It is horizontally and ripple cross laminated with a thickness on the order of cm's up to 1.5 meters and containing abundant plant material (example of fossilized tree trunk).

6. Channel-belt Internal Architecture

Several photomosaics of the fluvial channel-belt deposits were taken and analyzed for internal architecture. The interpreted bedding diagrams are shown beneath their respective photomosaics, in which zero to eighth order bounding surfaces are labeled.

6.1 Isolated Channel-belts

Description:

In total, only three of the eleven isolated channel-belts encased within finer floodplain sediments display easily observable internal architecture, represented with red boxes in figure 6.1.1.

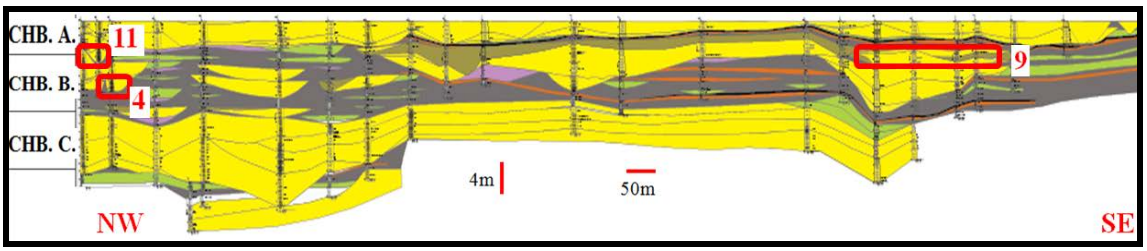

Figure 6.1.1 Cross section of research area highlighting the 3 out of 11 isolated channel-belts (red boxes) that demonstrated internal architecture.

Two of the three isolated channel-belts (CB4 & CB11) are located at the northern end of the cross section (Fig. 6.1.1). The upper part of figure 6.1.2 shows four channel-belt deposits. The lower three sand bodies are identified as isolated channel-belts. The uppermost sand body is identified as the amalgamated channel-belt. The interpreted bedding diagram (lower portion of Fig. 6.1.2) demonstrates internal architecture associated with the lower most (CB 4) and the top most (CB 11) isolated channel-belts. Both of these isolated channel-belts demonstrate a fining upward trend consisting of numerous dune-scale cross-bedded to ripple cross-laminated sandstone beds that are draped with mudstone. The thickness of the beds are on the order of centimeters, but are not greater than approximately 25 cm. The surfaces of the dipping beds can be traced laterally for a couple of meters before down-lapping or truncating against other surfaces. A noticeable difference between the beds of the two isolated channel-belts is the direction in which they dip. The lower most isolated channel-belt contains beds which accrete towards the right (~SE direction), whereas the upper most isolated channel-belt contains beds which accrete towards the left (~NW direction) (Fig. 6.1.2). Both of the isolated channel-belts demonstrate a NE paleocurrent direction (NE direction is into the cliff in Fig. 6.1.2), which is perpendicular to the direction in which the beds dip.

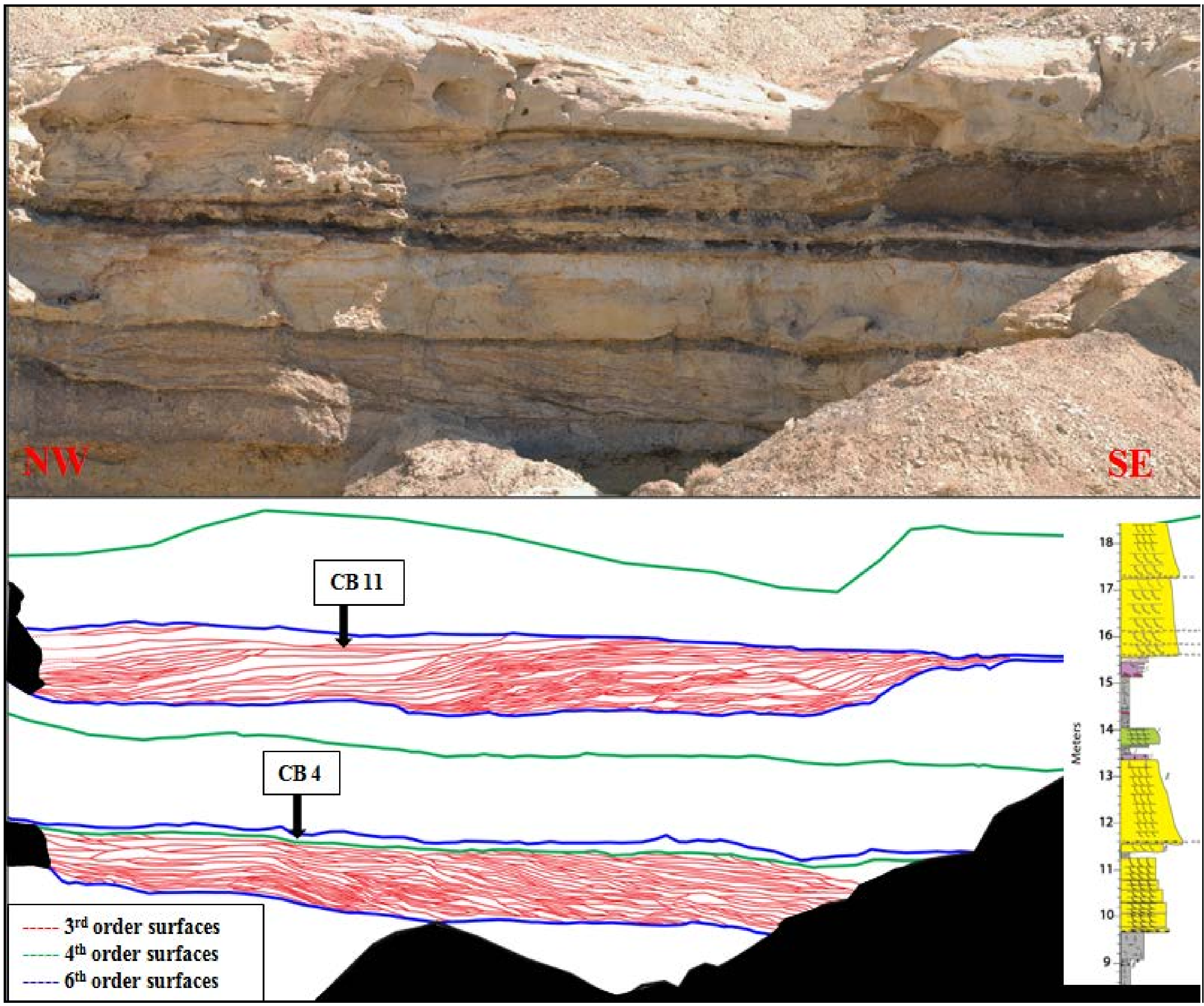

Figure 6.1.2 Photomosaic (above) and bedding diagram (below) of 2 isolated channel-belts at the northern end of the cross section demonstrating internal architecture. The lower isolated channel-belt (CB 4) has laterally accreting flood deposits dipping towards the right (~SE direction), while the top most isolated channel-belt (CB 11) has laterally accreting flood deposits dipping towards the left (~NW direction).

The third isolated channel-belt (CB 9) demonstrating internal architecture is located towards the southern end of the cross section (Fig. 6.1.1). At that location, the photomosaic of the outcrop demonstrates a total of 3 channel-belt deposits, the bottom two sandstone bodies are identified as isolated channel-belts, whereas the upper most sand body is identified as the amalgamated channel-belt (top portion of Fig. 6.1.3). The interpreted bedding diagram (lower portion of Fig. 6.1.3) documents internal architecture for only one of the two isolated channel-belts. The top isolated channel-belt (2nd channel-belt from the bottom) demonstrates a fining upward trend. The thickness of the beds are on the order of centimeters, but not greater than approximately 40 cm. The beds extend laterally, dipping towards the right (~SE direction), for a couple of meters prior to their surfaces down-lapping or truncating against other surfaces (Fig. 6.1.3). Paleocurrent direction is towards the NE (into the cliff in Fig. 6.1.3), which is perpendicular to the direction in which the beds dip.

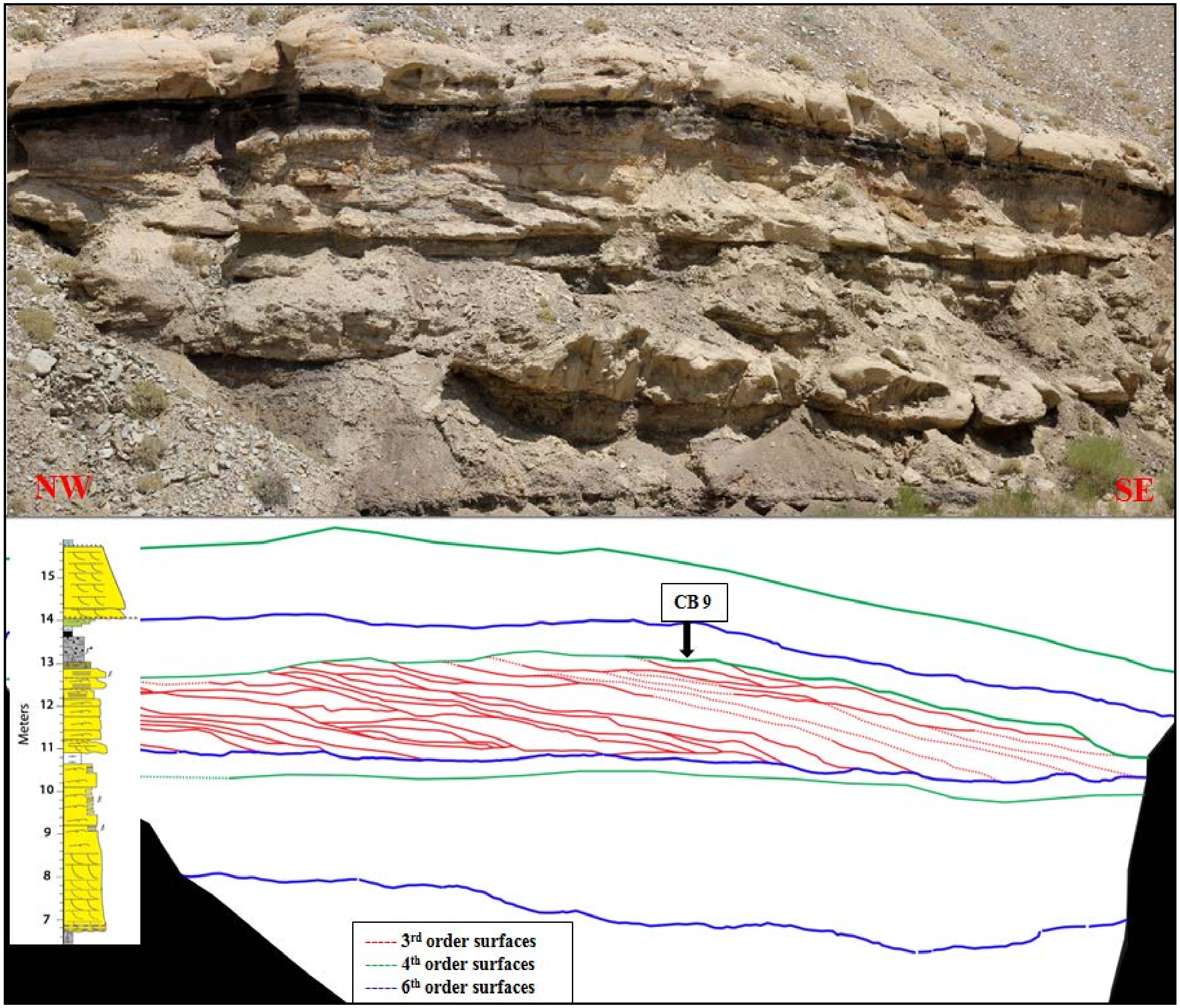

Figure 6.1.3 Photomosaic (above) and bedding diagram (below) of an isolated channel-belt towards the southern end of the cross section demonstrating internal architecture. The isolated channel-belt (CB 9) has laterally accreting flood deposits dipping towards the right (~SE direction).

Interpretation:

The sharp erosional contact between the base of each sandstone body and the underlying finer floodplain sediment, along with evidence of mud clasts in some locations, suggest that this is the erosional base associated with a channel-belt, or a 6th order surface. The fining upward trends associated with the dipping beds suggests that each bed represents depositional increments formed during distinct individual floods. The 3rd order surfaces in the bedding diagrams are therefore interpreted as laterally accreting flood deposits. The top of the last depositional event, or laterally accreting flood deposits, is interpreted as the bar top, or 4th order surfaces. Paleocurrent measurements recorded for all of the previously discussed isolated channel-belts indicate a NE paleoflow direction. This direction is perpendicular to the direction of accretion of the laterally accreting flood deposits, suggesting that these are laterally migrating point bars associated with fluvial meandering systems.

6.2 Amalgamated Channel-belt

Internal architecture could not be documented for the amalgamated channel-belt. This likely reflects the minimal grain size variation within the unit, as opposed to a unit with much more heterolithic facies and greater grain size variation in which internal architecture is easily depicted. The lack of finer grain facies suggest that the system was much more energetic, carrying coarser material. Additional features, such as the greater extent (width) of the sandstone body, its multistory nature, and low variation in paleocurrent measurements, suggest this is a low sinuosity possibly braided system.

7. Channel-belt Dimensions

The most noticeable difference between the amalgamated and isolated channel-belt deposits are their difference in channel-belt width. The lower portion of figure 7.1.1 is a map-view photo of the study area, in which different polygons are used to represent the different channel-belt deposits that could be correlated on opposite sides of Sweetwater Wash, according to their respective channel-belt margins. The upper portion of figure 7.1.1 is the cross section of the study area indicating their stratigraphic position, represented by their respective polygon color. The black arrows within individual polygons represent the paleocurrent direction of each individual fluvial system. Although the paleocurrent direction for all of the channel-belts is towards the NE, there is a clear difference in apparent (uncorrected) width (width of polygons), where the amalgamated channel-belt is much wider than all three isolated channel-belts.

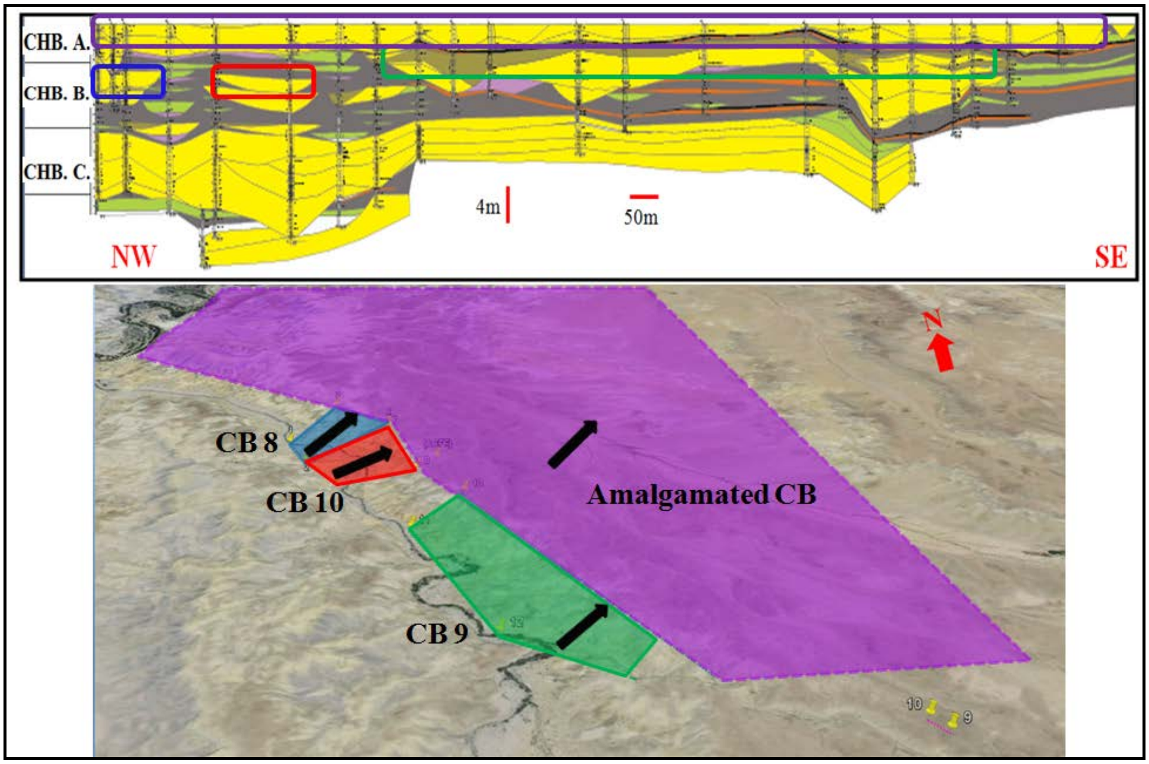

Figure 7.1.1 Cross section (above) and map-view (below). The polygons in the lower figure represent channel-belt margins which were able to be mapped out. The blue, red and green polygons represent isolated channel-belts with NE paleocurrent direction (black arrow within polygon). The purple polygon represents the amalgamated channel-belt, also with a NE paleocurrent direction. Channel-belts are represented on the cross section with their respective polygon color. From the map view picture, the significant difference in channel-belt width is clearly demonstrated.

In total, the apparent width and thickness of 12 channel-belts were obtained. 11 of the 12 channel-belts are isolated and are represented on the cross section with red polygons and numbers indicating their depositional order (Fig. 7.1.2). The amalgamated channel-belt was last to be deposited (12th channel-belt) and is represented on the cross section with a blue polygon (Fig. 7.1.2).

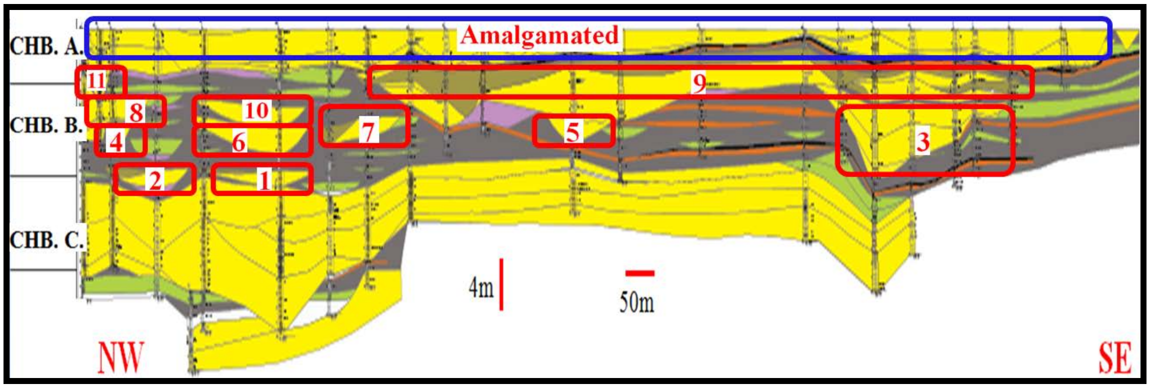

Figure 7.1.2 Picture demonstrating the 11 isolated channel-belts (red boxes) and amalgamated channel-belt (blue box) used to document channel-belt dimensions (width and thickness). Numbers within the boxes represent the order of deposition, beginning with number 1 (oldest) and ending with the amalgamated (youngest).

The corrected dimensions of all channel-belts are summarized in table 2. Note that the amalgamated channel-belt extends much farther than the study area, thus a minimum channel-belt width of ~2.8km and an average channel-belt thickness of 2.5m is used in all calculations. The calculated minimum width of the amalgamated channel-belt (in this study) is similar to the width documented by Zhu et al. (2012), recording a width of approximately 3km. Table 2 demonstrates the wide range of dimensions associated with the isolated channel-belts. They range from a minimum width of 40m up to a maximum width of 245m, and a minimum thickness of 1.1m up to a maximum thickness of 5m. Out of the eleven isolated channel-belts, two are multi-storey. Isolated channel-belt #3 consists of 3 storeys, whereas isolated channel-belt #9 is composed of 2 storeys. Therefore when averaging the dimensions of the isolated channel-belts, two different average values were calculated, one using all eleven isolated channel-belts, and another using only the single storey isolated channel-belts. Using all eleven isolated channel-belts an average channel-belt width of 135m and an average channel-belt thickness of 2.1m were obtained. Using only the single storey isolated channel-belts resulted in an average channel-belt width of 125m and an average channel-belt thickness of 1.57m. The amalgamated channel-belt, on the other hand, has a true minimum channel-belt width of ~2.8km and an average channel-belt thickness of 2.5m. The results indicate that the difference in thickness between the two types of channel-belts is not as significant as their difference in width. Figure 7.1.3 is a channel-belt width vs. thickness graph demonstrating that the width of the amalgamated channel-belt (width of ~2.8km), at a minimum, is an order of magnitude greater than the widest isolated channel-belt (width of ~245m).

Channel Belt	Outcrop Orientation	Paleocurrent Direction	Number of Storeys	Apparent Width (m)	Approximate True Width (m)	Thickness (m)	W/T Ratio
Isolated #1	340°	50°	1	203	190	1.1	175
Isolated #2	340°	45°	1	144	130	1.15	115
Isolated #3	350°	35°	3	338	245	5.0	50
Isolated #4	340°	85°	1	43	40	1.55	25
Isolated #5	323°	115°	1	118	55	1.8	30
Isolated #6	340°	100°	1	207	180	1.9	95
Isolated #7	340°	50°	1	143	135	1.45	95
Isolated #8	340°	90°	1	215	200	2.0	100
Isolated #9	340°	335°	2	1161	100	4.0	25
Isolated #10	340°	32°	1	189	150	1.4	110
Isolated #11	340°	30°	1	72	55	1.8	30
Average	N/A	N/A	All	276	135	2.1	65
Average	N/A	N/A	Single	148	125	1.57	80
Amalgamated	340°	20°	2-3	4400	2830	2.5	1130

Table 2. Table summarizing the outcrop orientation, paleocurrent direction, apparent width, true width, thickness, and W/T ratio for the amalgamated and isolated channel-belts.

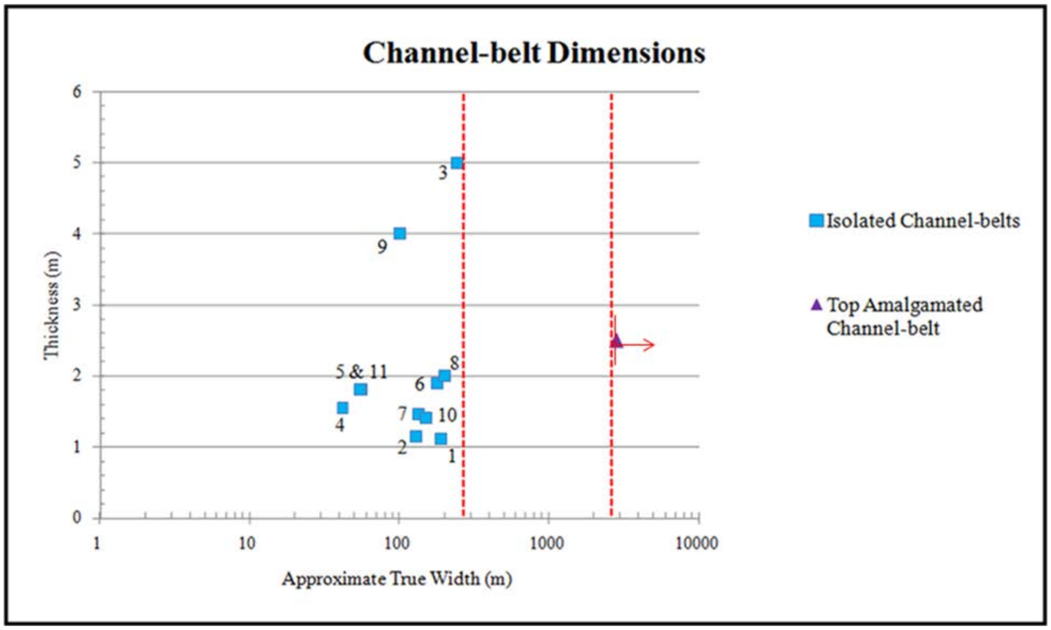

Figure 7.1.3 Channel-belt width vs. thickness graph demonstrating that the minimum width of the amalgamated channel-belt (purple triangle) is an order of magnitude greater than the isolated channel-belt (blue squares) with the greatest width.

Using channel-belt width and thickness, the W/T ratio was calculated for all 12 channel-belts, shown in table 2. The results indicate that the isolated channel-belts have W/T ratio ranging from a minimum value of 25, up to a maximum value of 175. When calculating the average W/T ratio using all eleven isolated channel-belts a value of 65 was obtained. Using only the single storey isolated channel-belts an average W/T ratio value of 80 was obtained. The amalgamated channel-belt, on the other hand, has a minimum W/T ratio value of 1,130. When values are compared, results once again indicate that the amalgamated channel-belt (minimum W/T ratio of 1,130), is an order of magnitude greater than the isolated channel-belt with the greatest W/T value (W/T ratio of 175) (Fig. 7.1.4).

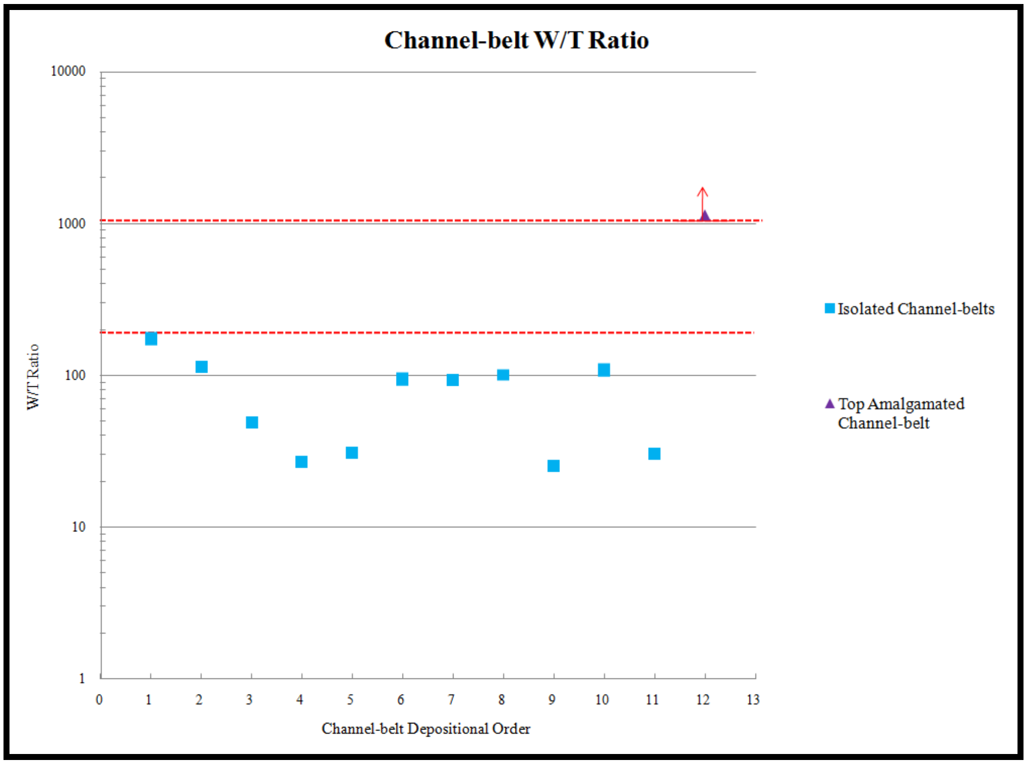

Figure 7.1.4 Graph of channel-belt width/thickness ratio demonstrating that the W/T ratio of the amalgamated channel-belt (purple triangle), at a minimum, is an order of magnitude greater than the isolated channel-belt (blue square)with the greatest W/T ratio.

In general, the thickness of a storey can be used as a proxy for channel depth. The single storey isolated channel-belts demonstrate a storey thickness ranging from 1.1m up to 2m, averaging a channel depth of about 1.57m and a maximum depth of 2m. The two multi-storey isolated channel-belts demonstrate individual storey thickness ranging from 0.8m up to 2.4m, averaging a channel depth of about 1.47m and a maximum depth of 2.4m. The top-most amalgamated channel-belt is also multi-storey. The storey thickness ranges from 0.4m up to 2.5m, averaging a channel depth of about 1.62m and a maximum depth of 2.5m. From this data, we can therefore conclude that the channels, regardless of being associated with the amalgamated or isolated channel-belts, never exceeded a depth of about 2.5m.

8. Discussion

8.1 Dimensions

In order to determine the fluvial style, the dimensions of the amalgamated and isolated channel-belts were compared to Gibling's (2006) study, as well as previous work in the Cretaceous Ferron Notom Delta by Li and Bhattacharya (in review).

In Gibling's (2006) study, the dimensions of more than 1500 fluvial bodies were documented and plotted on a width vs. thickness graph, in which three different polygons were created to represent the possible dimensions of braided/low sinuosity rivers, meandering rivers, and delta plain distributaries (Fig. 8.1.1). Although the polygons significantly overlap with one another in some places, a general idea can be obtained in regards to the style of the fluvial system. By documenting additional information (i.e. paleocurrent direction and associated facies) further possible distinctions can be made.

Figure 8.1.1 demonstrates Gibling's (2006) width vs. thickness graph in conjunction with the dimensions of the 11 isolated channel-belts (blue circles) as well as the amalgamated channel-belt (purple circle). The results demonstrate that the amalgamated channel-belt plots in a zone of overlap between the meandering river and the braided/low sinuosity river polygons. However, it has been documented that braided/low sinuosity river deposits commonly exceed a W/T ratio value of 100 and may even exceed 1000, forming broad to very broad sheets of sand (Gibling, 2006). The W/T ratio documented for the amalgamated channel-belt, at a minimum, is 1130. This, along with the low variations in paleocurrent measurements, are consistent with our interpretation that the amalgamated channel-belt deposit is most likely the result of a braided, low sinuosity system.

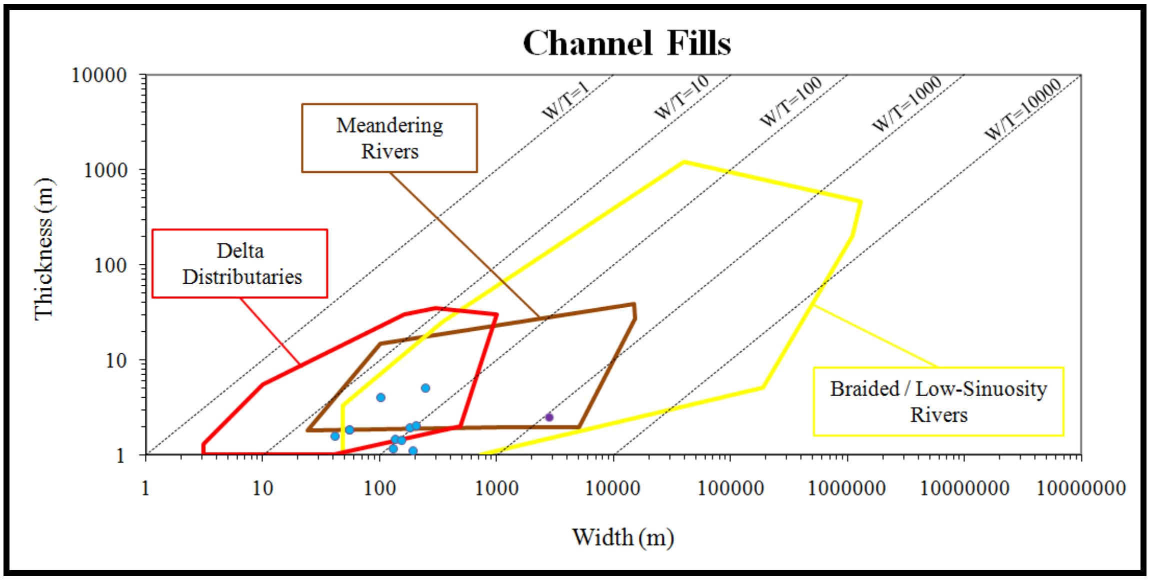

Figure 8.1.1 Width vs. thickness graph in which 3 different polygons demonstrate possible dimensions associated with braided/low sinuosity rivers (yellow polygon), meandering rivers (brown polygon), and delta distributaries (red polygon). The blue circles represent the isolated channel-belts and the purple circle represents the amalgamated channel-belt. See text for details.

The isolated channel-belts, plot within all three river polygons. The results indicate that 10 of the 11 isolated channel-belts plot within the braided/low sinuosity polygon, 9 of the 11 isolated channel-belts plot within the delta distributary polygon, and 6 of the 11 plot within the meandering polygon. However, the average W/T ratio for all 11 isolated channel-belts is 65, where only a few exceed the 100 mark (Table 2). This, along with the greater variation in paleocurrent measurements and documented laterally accreting flood deposits, indicate that the isolated channel-belts (possibly with the exception of 2) were most likely not the result of braided, low sinuosity systems.

Determining whether the isolated channel-belts are meandering or distributary becomes a bit more difficult. Attempting to use plan-form as a distinguishing feature is not very useful, due to the fact that laterally accreting surfaces, typically associated with point bars in meandering systems, have also been documented in distributary systems, indicating that distributary channels also migrate laterally to some degree (Bhattacharya, 2006; Gibling, 2006). The results in figure 8.1.1 demonstrate that a greater number of isolated channel-belts plot within the distributary polygon than in the meandering river polygon (9 vs. 6). The 6 isolated channel-belts that plot within the meandering river polygon are in a zone of overlap with the distributary polygon, where 4 of the 6 sit on the lower boundary of the meandering river polygon. The 2 isolated channel-belts that clearly plot within the meandering river polygon are the only multi-storey isolated channel-belts, which if divided and analyzed by individual storey, would plot closer to the lower boundary or even plot outside the meandering river polygon. This possibly indicates that the majority of the isolated channel-belts were distributary channels that demonstrated some degree of lateral migration.

To determine how similar the isolated channel-belts are to distributary systems, their dimensions were compared to distributary systems within the Cretaceous Ferron Notom Delta, documented by Li and Bhattacharya (in review), and represented with red circles in figure 8.1.2. They interpreted the larger channel-belts (channel-belts with greater width and thickness) to represent major delta plain distributary systems, whereas the smaller channel-belts (channel-belts with smaller width and thickness), were interpreted to represent smaller distributary branches (Li and Bhattacharya, in review).

The dimensions of the isolated channel-belts were plotted in conjunction with those documented by Li and Bhattacharya (in review), represented with blue squares in figure 8.1.2. From the results, we can see a clear and significant amount of overlap, indicating that the isolated channel-belts are very similar to and could very likely be distributary systems.

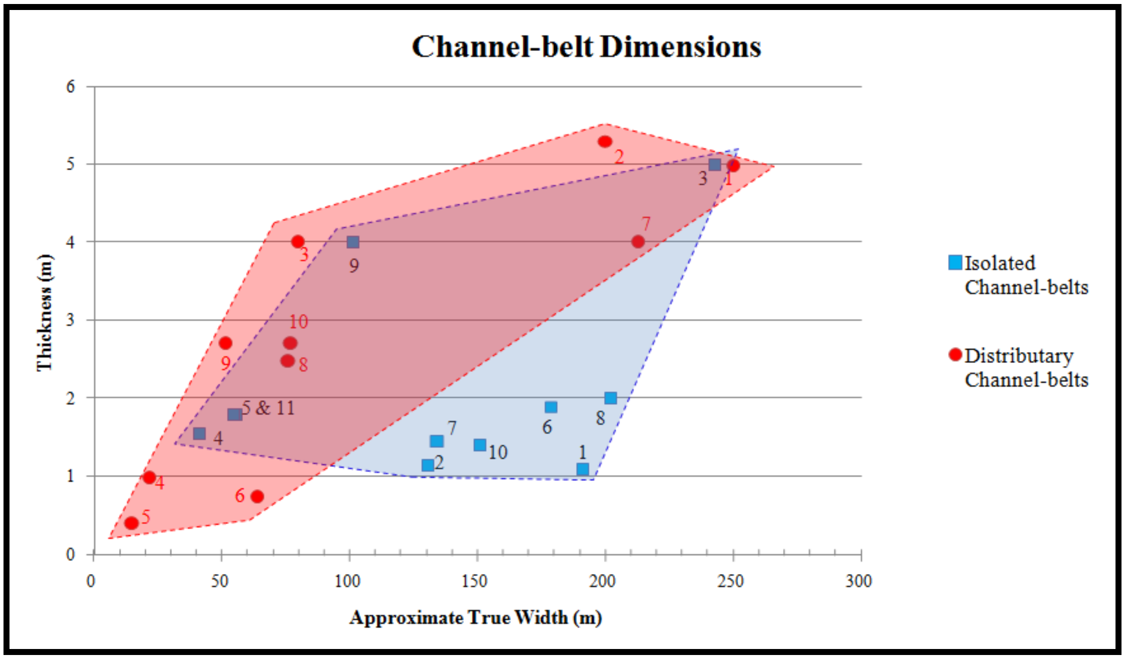

Figure 8.1.2 Width vs. thickness graph comparing the dimensions of the isolated channel-belts (blue squares within the blue polygon) to the dimensions of the distributary channel-belts (red circles within the green polygon). Results demonstrate significant amount of overlap between the distributary and isolated channel-belts. See text for details.

In terms of scale, Li et al. (2012) determined that the depth of the trunk channels in the Ferron range from 5-8m. In contrast, the scale of the channels documented in this study never exceed a depth of 2.5m, being half the size of trunk channel. Clearly these are much smaller scale channels, possibly indicating that they are associated with the distributary plain. In terms of facies, the distributary systems documented by Li and Bhattacharya (in review) are associated with paralic marine bay-fill facies, interpreted as lower delta-plain distributary systems. The isolated channel-belts in my study are completely encased in more proximal coals and floodplain sediment, clearly indicating that they are more landward. This suggest that the isolated channel-belts described in this study could possibly be upper delta-plain distributary systems, where the distributary form may be a result of regional and local avulsion patterns, given the observed increase in associated crevassing and floodplain lake deposits; evidence for flooding.

Using channel-belt dimensions presented in Gibling (2006), Li and Bhattacharya (in review), and Li et al. (2012) similar conclusions were obtained, suggesting that the amalgamated channel-belt was formed by braided, low sinuosity channels, whereas the isolated channel-belts were most likely laterally migrating meandering distributary channels along an upper delta plain.

8.2 Fluvial and Sequence Stratigraphic Models

Several fluvial facies models have been proposed in an attempt to address the distribution of fluvial deposits, suggesting different controls on the resulting sandstone/mudstone proportion (Friend, 1983; Bristow and Best, 1993; Shanley and McCabe, 1993; Wright and Marriott, 1993; Miall, 1996).

Earlier fluvial facies models, such as Friend (1983), suggest that the sandstone/mudstone proportion is a function of the fluvial plan-form, where a meandering plan-form is associated with low sandstone/mudstone proportions and the braided plan-form is associated with high sandstone/mudstone proportions (Fig. 8.2.1).

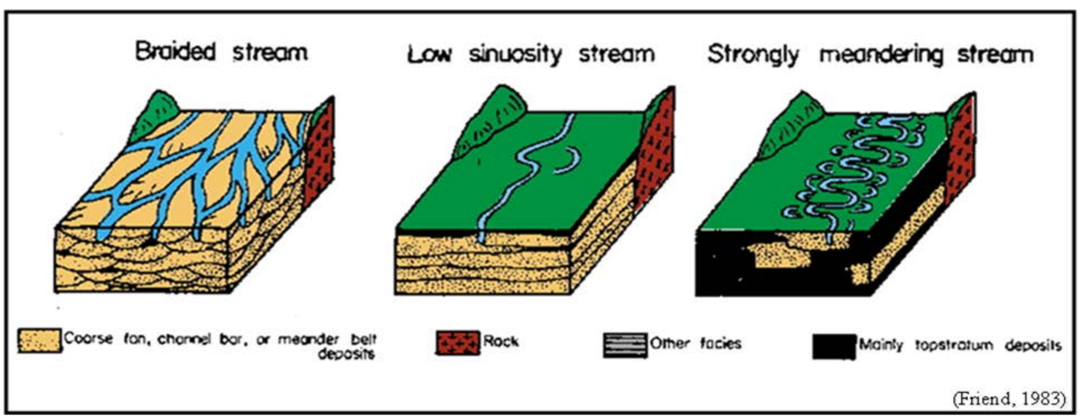

Figure 8.2.1 Schematic diagram by Friend (1983) demonstrating sandstone/mudstone proportion as a function of fluvial plan-form where the meandering plan-form is associated with low sandstone/mudstone proportions and the braided plan-form is associated with high sandstone/mudstone proportions.

Using internal bedding diagrams, we documented laterally accreting deposits in 3 of the 11 isolated channel-belts. The reason for the remaining 8 isolated channel-belts not showing clear internal architecture is unknown, but could be related to factors such as low variation in grain size, surface weathering, orientation of the outcrop to channel-belt, or channel-belt dimensions. The three isolated channel-belts with evidence of laterally accreting deposits demonstrate the lowest values in channel-belt width and W/T ratio (Fig. 8.2.2 & 8.2.3). The presence of laterally accreting deposits indicates that at least some of the isolated channel-belts (within a low sandstone/mudstone interval) were associated with laterally migrating point bars within meandering systems. The internal architecture for the amalgamated channel-belt (within a high sandstone/mudstone interval) could not be documented, however, channel-belt dimensions (Gibling, 2006) and low variation in paleocurrent measurements suggest it was most likely the result of a braided, low sinuosity system.

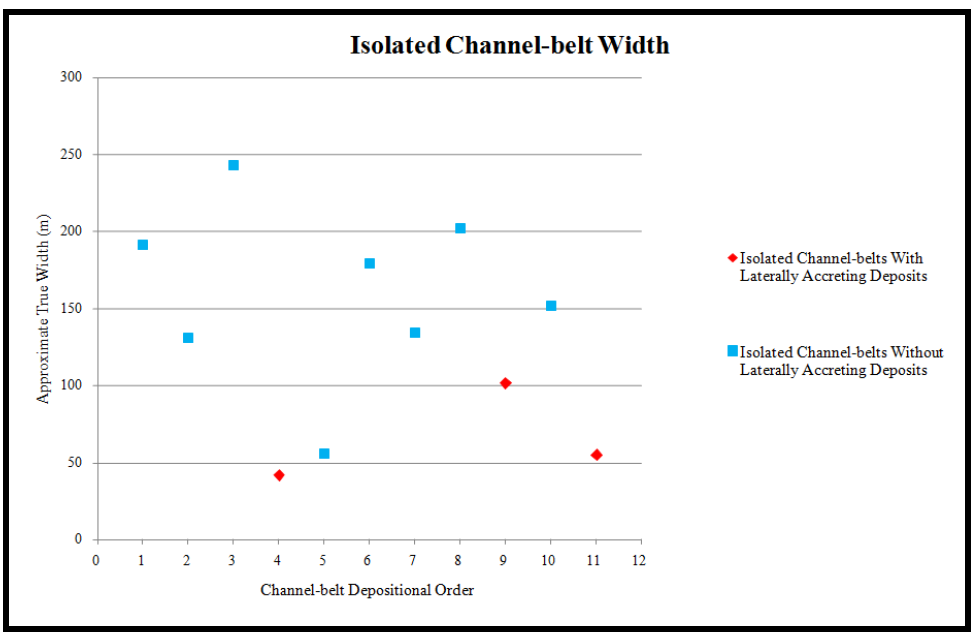

Figure 8.2.2 Graph demonstrating the isolated channel-belts with evidence of laterally accreting deposits (represented by the red diamonds) demonstrate the lowest channel-belt width values.

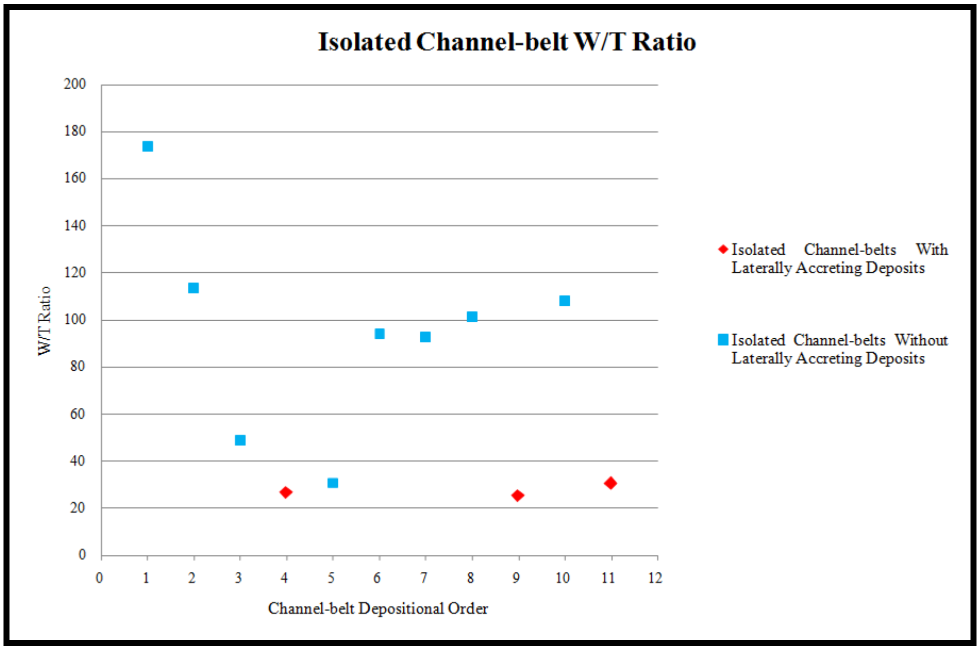

Figure 8.2.3 Graph demonstrating the isolated channel-belts with laterally accreting deposits (represented by the red diamonds) demonstrate the lowest values of channel-belt W/T ratios.

Our observations are consistent with the Friend (1983) fluvial facies model. Although his model matches the outcrop example in this study, we do not believe it is always applicable. This has been demonstrated in recent studies where a braided plan-form was documented within a low sandstone/mudstone interval (Willis, 1993; Adams and Bhattacharya, 2005), indicating that fluvial plan-form is not necessarily the dominant control of the sandstone/mudstone proportion.

Bristow and Best (1993) suggest that rather than plan-form determining the sandstone/mudstone proportion, it is actually a function of the rate of aggradation, lateral migration, and avulsion frequency (Fig. 8.2.4). By comparing channel-belt stacking patterns to Bristow and Best (1993) model, we can obtain an understanding regarding the dominant controls responsible for the resulting sandstone/mudstone proportion.

Field observations demonstrate that the top-most channel-belt (CHB. A) is amalgamated, consisting of 2 to 3 storeys that erode into one another, and much more laterally continuous. This sandstone body is coarser grain, ranging from coarse- to medium-grained sandstone, with no evidence of preserved intervening floodplain facies. The stacking pattern of this channel-belt best resemble that which is the result of low rates of aggradation, high rates of lateral migration, and low rates of avulsion frequency (Fig. 8.2.4).

In contrast, the underlying channel-belts (CHB. B) are much more isolated and narrower. These sandstone deposits are predominantly single storey, with only 2 of the 11 isolated channel-belts demonstrating a multi-storey nature. They are medium- to very fine-grained sandstones that are completely encased within finer floodplain deposits. The stacking pattern of these channel-belts best resemble those which result from low rates of lateral migration, high rates of aggradation, and high avulsion frequency (Fig. 8.2.4).

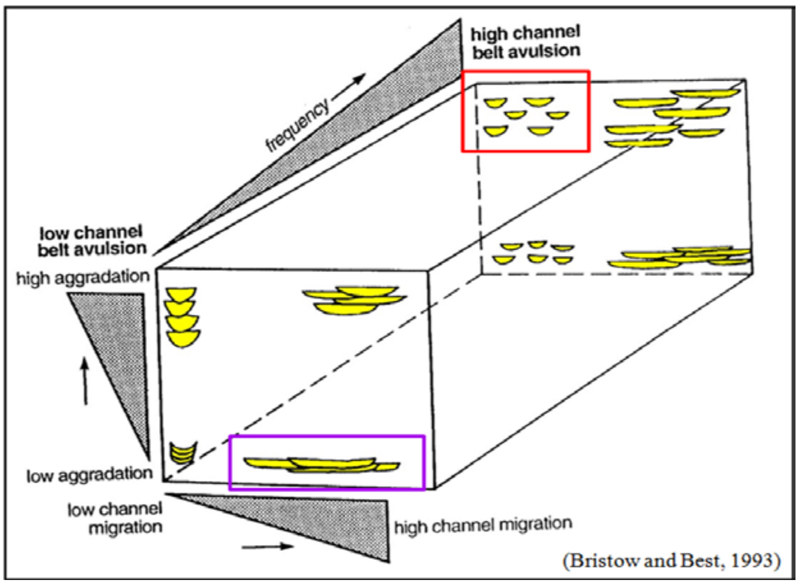

Figure 8.2.4 Schematic diagram proposed by Bristow and Best (1993) demonstrating the stacking relationships of fluvial deposits as a function of the rate of aggradation, lateral channel migration, and avulsion frequency. The purple polygon represents the geometry and stacking relationship closely related to the top amalgamated channel-belt (CHB. A) suggesting that it was the result of lower rates of aggradation, higher rates of lateral migration, and lower avulsion frequency. The red polygon represents the geometry and stacking relationship closely related to the isolated channel-belts (CHB. B) suggesting that it was the result of lower rates of lateral migration, higher rates of aggradation, and higher rates of avulsion frequency.

However, these three factors are not independent, they are influenced principally by changes in accommodation. We can relate these three factors back to changes in base level in the sense that an increase in base level creates accommodation, which increases the rate of aggradation. As the rate of aggradation increases, the slope or gradient of the river decreases, which in turn decreases the flow competence of the system to transport coarse sediment, erode its banks, and migrate laterally (Gibling, 2006). The increase in the rate of aggradation results in the buildup of the alluvial ridge (channel bed, levees, and floodplain), which therefore increases the probability for an avulsion (due to the low gradient advantage) (Gibling, 2006). The increase in base level/accommodation promotes an increase in the amount of sediment being stored in the floodplains (Wright and Marriott, 1993), leading to the creation of multiple isolated channel-belts.

This is consistent with field observations having documented laterally accreting deposits in three of the isolated channel-belts, suggesting a meandering style. Meandering systems result from lower channel-forming discharge and lower gradients. In this case, lower gradients may be attributed to the increase in the rate of aggradation associated with an increase in accommodation. Using dimensions and low variation in paleocurrent measurements, we interpreted the amalgamated channel-belt to be the result of a braided, low sinuosity system. Braided systems result from greater channel-forming discharge and higher gradients. The higher gradient may be attributed to the decrease in accommodation. We were also able to document a difference in grain size associated with the channel-belts, where the isolated channel-belts are finer grain. This can be attributed to a decrease in flow competence of the system, which may result from a gradient decrease related to an increase in accommodation. The isolated channel-belts are also much more narrower than the amalgamated channel-belt. This can be attributed to a decrease in the flow competence of the system to transport coarse sediment, erode its banks, and migrate laterally. It may also be attributed to the increase in the frequency of avulsion, where the system avulses periodically, decreasing the ability to migrate laterally. Both the decrease in flow competence and the increase in avulsion frequency could possibly be related in part back to an increase in accommodation. The isolated channel-belts are also completely encased by finer floodplain facies, whereas there is none associated with the amalgamated channel-belt. This can be attributed to an increase in avulsion frequency and less reworking of the floodplain, the response to an increase in the rate of aggradation which can be related back to an increase in accommodation (Gibling, 2006).

In terms of sequence stratigraphy, several models have been proposed associating the types of channel-belt distribution to different systems tract. In Shanley and McCabe (1993) model, they relate isolated channel-belts to the highstand systems tract, in which base level is relatively high. Their model also demonstrates that the only amalgamated channel-belts are those which are confined within the valley in the lowstand systems tract, in which base level in relatively low (Fig. 8.2.5). The model proposed by Wright and Marriott (1993), on the other hand, assign the isolated channel-belts to the transgressive systems tract, where base level is continually rising. Their model demonstrates amalgamated channel-belts to occur within the lowstand systems tract, however, they also show some degree of amalgamation or rejoining of channel-belts within the later part of the highstand systems tract (Fig. 8.2.6). Lastly, the model proposed by Miall (1996) assigns the isolated channel-belts to the transgressive and early highstand systems tract, whereas the amalgamated channel-belts are assigned to the late highstand as well as the lowstand systems tract (Fig. 8.2.7).

From these sequence stratigraphic models, one uniform observation can be made or agreed upon. The observed distribution of isolated channel-belts occur during relative increase accommodation, and that of amalgamated channel-belts occur during relative decrease in accommodation. Hence, the rate of aggradation, avulsion frequency, and lateral migration in fluvial systems are linked to changes in accommodation.

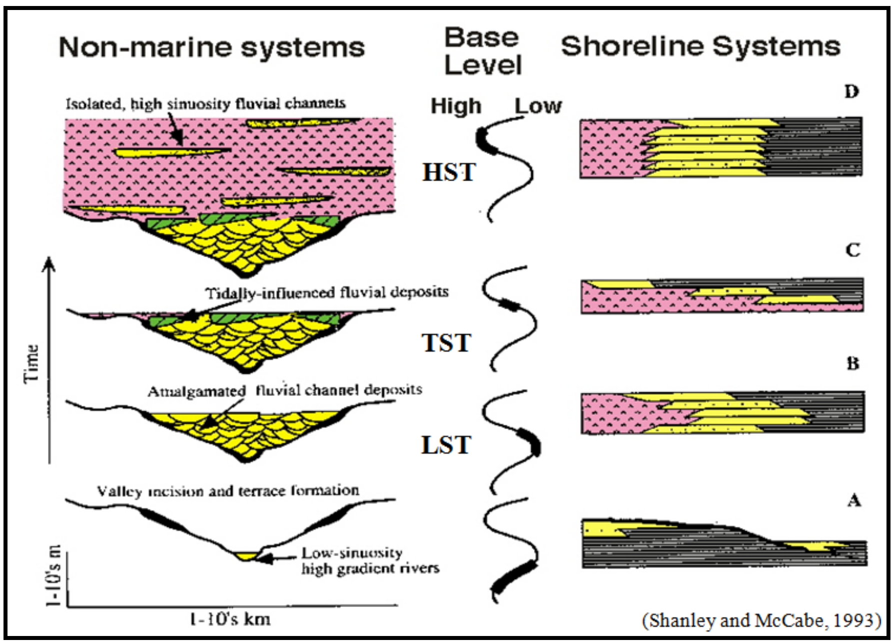

Figure 8.2.5 Schematic diagram by Shanley and McCabe (1993) illustrating the relationship between channel-belt distribution and changes in base level. During the LST, base level fall reduces and begins to rise slowly resulting in amalgamated fluvial deposits within the valley. During the TST, the increasing base level result in tidally influenced fluvial deposits. During the HST, the reduced rate in base level rise result in isolated, highly sinuous fluvial deposits.

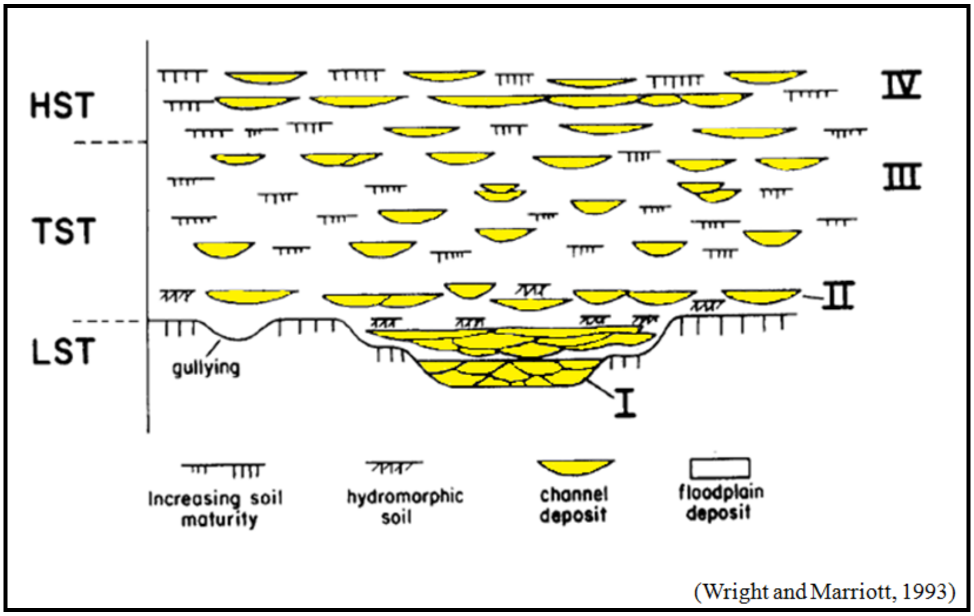

Figure 8.2.6 Schematic diagram by Wright and Marriott (1993) illustrating the relationship between channel-belt distribution and changes in base level. During the LST, accommodation is low and the increased gradients will result in low sinuosity deposits within the valley. During the TST, the rate of accommodation increases, favoring high levels of storage of floodplain sediment resulting in isolated channel-belts. During the HST, accommodation is reduced resulting in higher rates of floodplain reworking and rejoining of channel-belts.

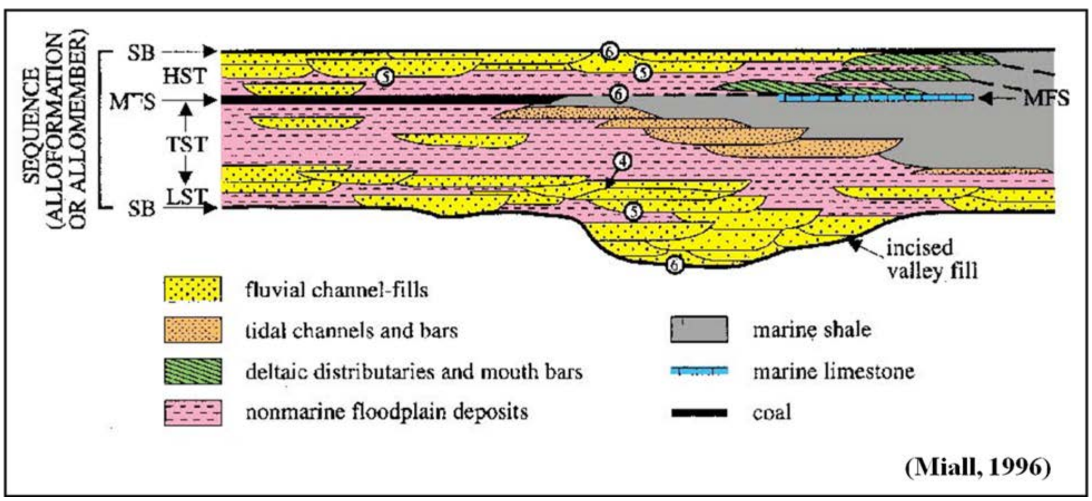

Figure 8.2.7 Schematic diagram by Miall (1996) illustrating the relationship between channel-belt distribution and changes in base level. During the LST, accommodation is low, resulting in amalgamated deposits aggrading within the valley. During the TST there's an increase in the rate of accommodation resulting in an increase of isolated sandstone bodies. During the HST, the rate of accommodation increase slows down, resulting in isolated bodies in the early stage which is then followed by rejoining of sandstone bodies in the later stage.

From field observations we were able to determine that the resulting sandstone/mudstone proportion, is not necessarily determined by the fluvial plan-form, as predicted by Friend (1983), but most likely determined by the rate of aggradation, avulsion frequency, and lateral migration, as predicted by Bristow and Best (1993). These factors, however, are linked to changes in accommodation, as predicted by Shanley and McCabe (1993), Wright and Marriott (1993), and Miall (1996).

8.3 Channel-belt Dimensions in Sequence Stratigraphy

Previously discussed models (Shanley and McCabe, 1993; Wright and Marriott, 1993; Miall, 1996) suggest that non-marine sequences show organized and systematic changes in stacking patterns where high sandstone/mudstone intervals are typically associated with the confinement of channel-belts, and related to the sequence boundary within the lowstand systems tract. In the low sandstone/mudstone interval there is an increase in marine/tidal influence, associated with the transgressive systems tract in which coal and/or limestone beds may indicate the point of maximum flooding or marine transgression. The transition into the highstand systems tract can be indicated by a greater degree of amalgamation and increasing sandstone/mudstone proportions.

In addition, Wright and Marriott (1993) suggested that there may be an organized vertical succession of paleosols in which the humidity of the soil increases going from the lowstand to the transgressive systems tract, and decreases going towards the highstand systems tract. Although it is difficult to define parasequences in non-marine successions, in this study, as well as Famubode (in prep), we attempt to use channel-belt dimensions, coal beds, and pedostratigraphic units to define the basic cyclicity of a non-marine section. Although the paleosol variability will not be discussed in this study, the vertical stacking of channel-belts and their dimensions are analyzed for possible systematic variations.

There have been a number of studies that have documented variations in dimensions along the longitudinal (downstream) profile of distributary systems. Gouw and Berendsen (2007), Makaske et al. (2007), and Tornqvist et al. (1993) recorded dimensions of distributary channel-belts in the Rhine-Meuse Delta and reached similar conclusions. They documented a downstream decrease in channel-belt width, as well as a downstream decrease in channel-belt W/T ratio. They concluded that the downstream variations are related to factors such as bank erodibility and stream power, where the ability of a system to laterally migrate decreases with decreasing stream power and/or bank erodability (Gouw and Berendsen, 2007). Assuming that these trends are applicable to all distributary systems, smaller scale channel-belts may be seen in more distal locations (basinward), where an increase in accommodation could possibly be represented as an upwards decrease in channel-belt dimension.

In order to address the possibility of vertical trends in dimensions, the channel-belts were arranged according to order of deposition. Figure 8.3.1 and 8.3.2 are plots demonstrating the changes in width and W/T ratio for the channel-belts, where channel-belt #0 represents the bottom-most amalgamated channel-belt deposit (stratigraphically the oldest). Results for channel-belt width suggest there is no significant change associated with the transition from the lowest amalgamated to the isolated channel-belt deposits, however, we do see a drastic increase in channel-belt width associated with the top-most amalgamated deposit (Fig. 8.3.1). When analyzing the results for W/T ratios we see a small increase between the lowest amalgamated and the overlying isolated channel-belt deposits. This is, however, a significant increase in W/T ratio between the isolated channel-belts and the top-most amalgamated channel-belt (Fig. 8.3.2). Although these general inferences can be made from the results, the obtained "R-squared" values are very low, suggesting that there is not a statistically significant correlation between the changes in channel-belt dimensions to their positioning within a sequence. Similar conclusions were obtained for similar analysis carried out for Zhu et al. (2012) regional cross section of the Ferron (Fig. 2.4), being unable to document any systematic trends in channel-belt dimensions.

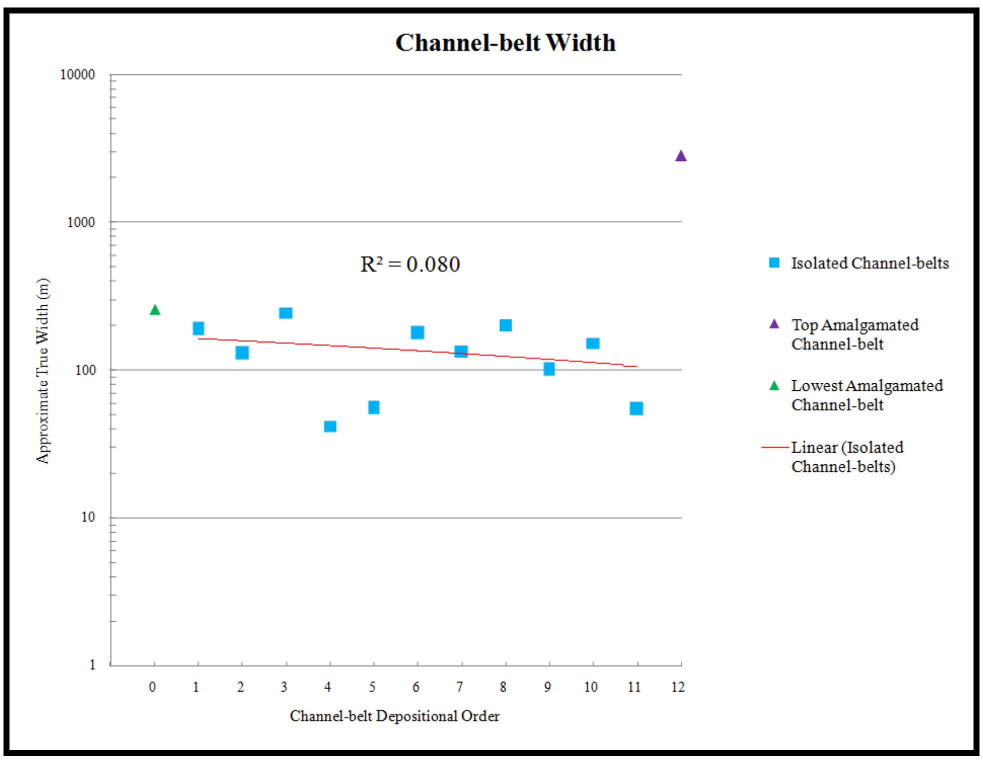

Figure 8.3.1 Graph demonstrating changes in channel-belt width. Results indicate that there's no statistically significant change associated with the transition from the lowest amalgamated to the isolated channel-belt deposits. This is then followed by a drastic increase in channel-belt width associated with the top most amalgamated channel-belt deposit.

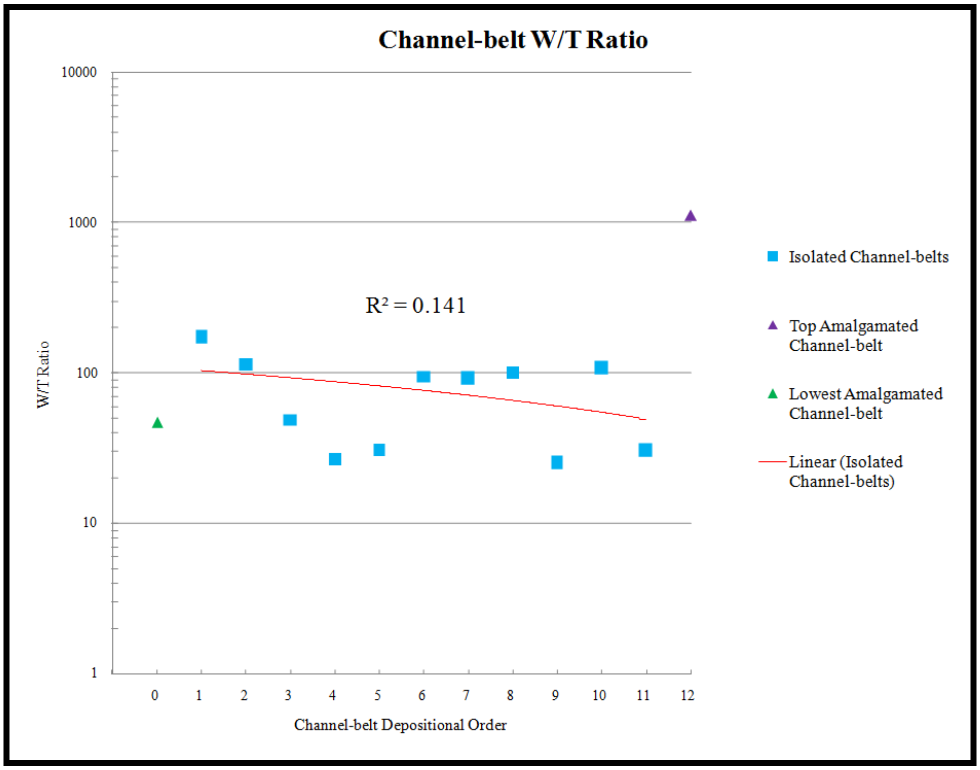

Figure 8.3.2 Graph demonstrating changes in channel-belt W/T ratios. Results indicate a small increase in W/T ratio associated with the transition from the lowest amalgamated to the isolated channel-belt deposits. This is then followed by an abrupt or drastic increase in W/T ratio associated with the top most amalgamated channel-belt deposit.

Although there appears to be no consistent systematic change in channel-belt dimensions, there does appear to be a systematic change in the sandstone/mudstone proportion, consistent with previously discussed sequence stratigraphic models. The regional cross sections (Fig. 2.3 & 2.4) demonstrate that the deposits confined within the valley are amalgamated, resulting in high sandstone/mudstone proportions, making up the lowstand systems tract (Shanley and McCabe, 1993; Wright and Marriott, 1993; Miall, 1996). The regional cross sections, as well as the cross section from our study area, demonstrate that the out of valley deposits (post valley fill) are predominantly mudstones with the presence of isolated, highly sinuous deposits. This results in low sandstone/mudstone proportions, thought to represent the transgressive to early highstand systems tract (Shanley and McCabe, 1993; Wright and Marriott, 1993; Miall, 1996). Within the middle to upper part of the low sandstone/mudstone interval, we see the presence of coal horizons. Coals are believed to represent a rise in the water table and are used as flooding surfaces in non-marine sequence stratigraphy (van den Bergh and Garrison, 1996; Garrison and van den Bergh, 2004; Davies et al., 2006). This is similar to Miall (1996) non-marine sequence stratigraphic model where a coal horizon is used to represent the maximum flooding surface, representing the turnaround point between the transgressive and highstand systems tract. Lastly, the regional cross sections as well as the cross section from our study area, demonstrate an increase in the degree of amalgamation, where channel-belt deposits are of low sinuosity. This results in high sandstone/mudstone proportions, and are thought to represent the depositional late highstand systems tract (Wright and Marriott, 1993; Miall, 1996).

9. Conclusions

Using documented channel-belt dimensions and comparing them to dimensions in the literature, we were able to determine that the upper amalgamated channel-belt was the result of braided, low sinuosity channels, whereas the isolated channel-belts were most likely laterally migrating meandering distributary channels along an upper delta-plain.

The muddier isolated systems appear to show a tendency for meandering, whereas coarser amalgamated systems show a tendency for braiding. Although we do not believe this is the only determining factor, field observations from this study are consistent with models suggesting that sandstone/mudstone proportions are related to the river plan-form.

The variations in the scale of channel-belts indicate that smaller isolated channel-belts and larger amalgamated channel-belt are consistent with stacking patterns predicted in models which relate sandstone/mudstone proportions to changes in the rate of aggradation, lateral migration, and avulsion frequency. These factors can be linked to changes in accommodation.

Using channel-belt dimensions within a vertical fluvial succession, we determined that there is not a consistent systematic change in channel-belt dimensions associating the changes in dimensions to their positioning within a sequence. However, there does appear to be a systematic change in the sandstone/mudstone proportion, where confined valley fill deposits are amalgamated with high sandstone/mudstone proportions, making up the LST. The out of valley deposits are predominantly mudstone, low sandstone/mudstone proportion, with isolated, highly sinuous deposits making up the TST to early HST. This is then followed by amalgamated, low sinuosity channel-belt deposits with greater sandstone/mudstone proportions, believed to represent the late HST.

References

Armstrong, R. L., 1968, Sevier orogenic belt in Nevada and Utah: Geological Society of America Bulletin, v. 79, p. 429-458.

Adams, M.M. and Bhattacharya, J.P., 2005, No change in fluvial style across a sequence boundary, Cretaceous Blackhawk and Castlegate Formations of central Utah, U.S.A.: Journal of Sedimentary Research, v. 75, p. 1038-1051.

Bhattacharya, J.P. and Tye, R.S., 2004, Searching for modern Ferron analogs and application to subsurface interpretation: AAPG Studies in Geology 50, p. 39-57.

Bhattacharya, J.P., 2006, Deltas: SEPM Special Publication No. 84, p. 237-292.

Bridge, J.S, 2003, Rivers and Floodplains: Forms, Processes, and Sedimentary Record: Blackwell Science: Oxford U.K., 491 p.

Bridge, J.S., 2006, Fluvial facies models: Recent developments *in* Facies Models Revisited. SEPM Special Publication No. 84, p. 83-168.

Bristow, C.S. and Best, J.L., 1993, Braided rivers: perspective and problems: Geologic Society Special Publications, v. 75, p. 1-11.

Davies, D.K., Williams, B.P.J., and Vessell, R.K., 1991, Reservoir models for meandering and straight fluvial channels; Examples from the Travis Peak Formation, East Texas: Transactions-Gulf Coast Association of Geological Societies, v. 42, p. 152-174.

Davies, N.S. and Gibling, M.R., 2010, Paleozoic vegetation and the Siluro-Devonian rise of fluvial lateral accretion sets: Geological Society of America Bulletin, v. 38, p. 51-54.

Davies, R., Howell, J., Boyd, R., Flint, S., and Diessel, C., 2004, High-resolution sequence-stratigraphic correlation between shallow-marine and terrestrial strata: Examples from the Sunnyside Member of the Cretaceous Blackhawk Formation, Book Cliffs, eastern Utah: American Association of Petroleum Geologists Bulletin, v. 90, p. 1121-1140.

Donselaar, M.E. and Overeem, I., 2008, Connectivity of fluvial point-bar deposits: An example from the Miocene Huesca fluvial fan, Ebro Basin, Spain: American Association of Petroleum Geologists Bulletin, v. 92, p. 1109-1129.

Famubode, O.A., Floodplain paleosols and their stratigraphic significance Cretaceous Ferron-Notom Delta, Utah. (Ph.D. Dissertation in prep).

Friend, P.F., Slater, M.J., and Williams, R.C., 1979, Vertical and lateral building of river sandstone bodies, Ebro Basin, Spain: Journal of the Geological Society, v. 136, p. 39-46.

Friend, P.F., 1983, Towards the field classification of alluvial architecture or sequence: Spec. Publs Int. Ass. Sediment, v. 6, p. 345-354.

Gardner, M.H., 1995, Tectonic and eustatic controls on the strata architecture of mid-Cretaceous stratigraphic sequence, central western interior foreland basin of North America: in S.L. Dorobek and G.M. Ross, eds., Stratigraphic Evolution of Foreland Basins: Society for Sedimentary Geology Special Publications 52, p. 243-281.

Garrison, J.R. and van den Bergh, T.C., 2004, High resolution depositional sequence stratigraphy of the Upper Ferron Sandstone Last Chance Delta: An application of coal zone stratigraphy: in T.C. Chidsey, R.D. Adams, T.H. Morris, eds., Regional to Wellbore Analog for Fluvial-Deltaic Reservoir Modeling; the Ferron Sandstone of Utah: American Association of Petroleum Geologists Studies in Geology 50, p. 125-192.

Gibling, M.R., 2006, Width and thickness of fluvial channel bodies and valley fills in the geological record: A literature compilation and classification: Journal of Sedimentary Research, v. 76, p. 731-770.

Gouw, M.J.P. and Berendsen, H.J.A., 2007, Variability of channel-belt dimensions and the consequences for alluvial architecture: observations from the Holocene Rhine-Meuse Delta (The Netherlands) and lower Mississippi valley (U.S.A.): Journal of Sedimentary Research, v. 77, p. 124-138.

Kauffman, E.G., 1984, Paleobiogeography and evolutionary response dynamic in the Cretaceous western interior seaway of North America: Geological Association of Canada Special Paper 27, p. 273-306.

Li, Y. and Bhattacharya, J.P., in review, Facies architecture, branching pattern, and paleodischarge of a lower delta-plain distributary channel system in the Cretaceous Ferron Notom delta, southern Utah, U.S.A.: Sedimentology.

Li, W., Bhattacharya, J.P., and Zhu, Y., 2012, Stratigraphic uncertainty in sparse versus rich data sets in a fluvial-deltaic outcrop analog: Ferron Notom delta in the Henry Mountains region, southern Utah: American Association of Petroleum Geologists Bulletin, v. 96, no. 3, p. 415-438.

Li, W., Bhattacharya, J.P., and Campbell, C., 2010, Temporal evolution of fluvial style in a compound incised-valley fill, Ferron "Notom Delta," Henry Mountains region, Utah (U.S.A.): Journal of Sedimentary Research, v. 80, p. 529-549.

Makaske, B., Berendsen, H.J.A., and Van Ree, M.H.M., 2007, Middle Holocene avulsion-belt deposits in the central Rhine-Meuse Delta, The Netherlands: Journal of Sedimentary Research, v. 77, p. 110-123.

Miall, A.D., 1992, Alluvial deposits: in Walker, R.G., and James, N.P., eds., Facies Models: Geological Association of Canada, p. 119-142.

Miall, A.D., 1996, The Geology of Fluvial Deposits; Sedimentary Facies, Basin Analysis, and Petroleum Geology: Springer-Verlag: Berlin, 582 p.

Miall, A.D., 1997, The Geology of Stratigraphic Sequences: Springer-Verlag: Berlin, 433 p.

Peterson, F. and Ryder, R.T., 1975, Cretaceous rocks in the Henry Mountains region, Utah and their relation to neighboring regions: in J.E. Fassett and S.A. Wengerd, eds., Canyonlands Country: Four Corners Geological Society Guidebook, 8th Field Conference, p. 167-189.

Ryer, T.A. and Anderson, P.B., 2004, Facies of the Ferron Sandstone, East-Central Utah: American Association of Petroleum Geologists Studies in Geology 50, p. 59-78.

Shanley, K.W. and McCabe, P.J., 1991, Predicting facies architecture through sequence stratigraphy- An example from the Kaiparowits Plateau, Utah: Geology, v. 19, p. 742-745.

Shanley, K.W. and McCabe, P.J., 1993, Alluvial architecture in a sequence stratigraphic framework: A case history from the Upper Cretaceous of southern Utah, U.S.A.: In S. Flint and I. Bryant, eds., Quantitative modeling of clastic hydrocarbon reservoirs and outcrop analogues: International Association of Sedimentologist Special Publication 15, p. 21-55.

Shanley, K.W. and McCabe, P.J., 1994, Perspectives on the sequence stratigraphy of continental strata: American Association of Petroleum Geologists Bulletin, v. 78, p. 544–568.

Tornqvist, T.E., Van Ree, M.H.M., and Faessen, E.L.J.H., 1993, Longitudinal facies architectural changes of a middle Holocene anastomosing distributary system (Rhine-Meuse delta, central Netherlands): Sedimentary Geology, v. 85, p. 203-219.

Tye, R.S., Bhattacharya, J.P., Lorsong, J.A., Sindelar, S.T., Knock, D.G., Puls, D.D., and Levinson, R.A., 1999, Geology and stratigraphy of fluvio-deltaic deposits in the Ivishak Formation: Applications for development of Prudhoe Bay Field, Alaska: American Association of Petroleum Geologists Bulletin, v. 83, p. 1586-1623.

van den Bergh, T.C.V. and Garrison, J.R., 1996, Channel-belt architecture and geometry - A function of depositional parasequence set stacking pattern, Ferron sandstone, east-central Utah: American Association of Petroleum Geologists Rocky Mountain Section Meeting, expanded abstracts volume, Montana Geological Society, p. 37-42.

Van Wagoner, J.C., Mitchum, R.M., Campion, K.M., and Rahmanian, V.D., 1990, Siliciclastic Sequence Stratigraphy in Well Logs, Cores, and Outcrop: American Association of Petroleum Geologists, Method in Exploration Series no.7, 55 p.

Willis, B., 1993, Ancient river systems in the Himalayan foredeep, Chinji Village area, Northern Pakistan: Sedimentary Geology, v. 88, p. 1-76.

Wright, V.P. and Marriott, S.B., 1993, The sequence stratigraphy of fluvial depositional systems: the role of floodplain sediment storage: Sedimentary Geology, v. 86, p. 203-210.

Zhu, Y., Bhattacharya, J.P., Li, W., Lapen, T.J., Jicha, B.R., and Singer, B.S., 2012, Milankovitch-scale sequence stratigraphy and stepped forced regression of the Turonian Ferron Notom deltaic complex, south-central Utah, U.S.A.: Journal of Sedimentary Research, v.82, p. 723-746.